ResearchGate

See discussions, stats, and author profiles for this publication at: https://www.researchgate.net/publication/220121941

Design and Kinematic Modeling of Constant Curvature Continuum Robots: A Review

Article *in* The International Journal of Robotics Research · November 2010

DOI: 10.1177/0278364910368147 · Source: DBLP

CITATIONS
1,551

READS
10,919

2 authors, including:

Bryan A. Jones
Mississippi State University
41 PUBLICATIONS **4,684** CITATIONS

SEE PROFILE

Some of the authors of this publication are also working on these related projects:

writing to learn to program View project

A Modular Plugin-in Architecture for CodeChat View project

All content following this page was uploaded by Bryan A. Jones on 23 September 2015.

The user has requested enhancement of the downloaded file.

Design and Kinematic Modeling of Constant Curvature Continuum Robots: A Review

Robert J. Webster III and Bryan A. Jones

Abstract

Continuum robotics has rapidly become a rich and diverse area of research, with many designs and applications demonstrated. Despite this diversity in form and purpose, there exists remarkable similarity in the fundamental simplified kinematic models that have been applied to continuum robots. However, this can easily be obscured – especially to a newcomer to the field – by the different applications, coordinate frame choices, and analytical formalisms employed. In this paper we review several modeling approaches in a common frame and notational convention, illustrating that for piecewise constant curvature, they produce identical results. This discussion elucidates what has been articulated in different ways by a number of researchers in the past several years, namely that that constant curvature kinematics can be considered as consisting of two separate submappings – one that is general and applies to all continuum robots, and another that is robot-specific. These mappings are then developed both for the single-section and for the multi-section case. Similarly, we discuss the decomposition of differential kinematics (the robot's Jacobian) into robot-specific and robot-independent portions. The paper concludes with a perspective on several of the themes of current research that are shaping the future of continuum robotics.

1 Introduction

Biology has inspired researchers in many ways, and there are few fields of study where this is more clearly evident than in continuum robotics. The incredible capabilities for locomotion, manipulation, and dexterity in cluttered environments exhibited by snakes, elephant's trunks, tongues, and octopus tentacles have naturally inspired researchers to work toward recreating their capabilities in electromechanical devices. Recent progress toward this end has made modern continuum robotics a rapidly expanding area of research which promises to extend the use of robots into many new environments where they have not traditionally been applicable. A continuum robot can be defined as a continuously bending, infinite-degree-of-freedom robot with an elastic structure (see Figure 1 for examples). Continuum robots are thus related to, but distinct from, hyperredundant robots which consist of (finitely) many short, rigid links (see Figure 1 for an example). Use of continuum robots in practical applications requires models of robot shape and motion. Such models must necessarily be more complex than those of traditional robots, which have a small number of rigid links. The purpose of this paper is to provide an overview of the state of the art in continuum robot design and forward and differential kinematic modeling for both single-section and multi-section manipulators.

Our review is motivated by several factors. First, several years have elapsed since the most often cited reviews of continuum robotics [37, 77], during which many important advancements have been made. This has motivated two new review papers within the past year focusing on locomotion of mobile snake-like robots [97] and the biological inspiration and design of soft (particularly pneumatic) continuum robots [99]. These are complementary to our current review of constant-curvature kinematics, with little overlap. Secondly, the diversity of applications (see Section 2) for continuum robots leads to a widely distributed literature, which can make it challenging for newcomers to the field to collect all relevant results expeditiously. An additional layer of complexity in interpreting results is the variety of mathematical formalisms and coordinate frame choices employed. Similarly, the distinction between robot-specific and robot-independent results can be subtle, which has led to some

of the same results being re-demonstrated in a number of papers, including the authors' own work. Interestingly and productively, if it is clear that multiple approaches can achieve the same results, this re-demonstration provides a variety of techniques for continuum robot kinematics, each of which may have unique advantages for future modeling, design, and real-time implementation efforts. Furthermore, the results in this paper will be particularly useful for a newcomer to the field of continuum robotics who desires simple and straightforward answers to questions such as "What is known about continuum robots?" and "How can I describe the shape and motion of my new continuum robot design?"

Unlike kinematics for traditional rigid-link robots where the pose of any point on the robot can be fully defined (in closed form) by link lengths and joint angles, the inherent compliance of continuum robots requires consideration of elasticity. To accurately define the pose of points of interest on the robot (including its end effector), one must characterize forces and moments applied to the robot by both its own actuators and the external environment. The most general models available for this (e.g. [45, 33, 98, 81, 85, 30, 19, 47]) do not do so in closed form. Instead, they are evaluated numerically to compute statics or dynamics in lieu of forward kinematics. Although some preliminary work exists in the real-time evaluation of these systems [47], it is not yet clear whether such results can be used to develop real-time Jacobians or can otherwise be applied to facilitate closed-loop control of continuum robots in a wide variety of applications.

Thus, both before and after the development of these general models, researchers have sought suitable simplifying assumptions and approximations that can be accurate enough for practical implementation and are more analytically tractable. One approach begins by describing the space curves desired, then fitting the physical robot (as nearly as possible) to these theoretical curves (see e.g. [3]). For example, clothoid curves have been proposed based on careful observations of biological snakes and are particularly useful for mimicking biological snake locomotion [37, 39]. Extending the basic approach of fitting the physical manipulator to analytically desirable mathematical curves, work in [20] defines a curve as the product of a Bessel function with sines and cosines which enables a modal approach

to inverse kinematics. Similarly, wavelets are applied in [32] to describe the shape of a continuum robot.

An alternative simplifying approach that permits closed-form kinematics and facilitates closed-form Jacobian formulation is to approximate the robot as a series of mutually tangent constant curvature arcs ("piecewise constant curvature"). While most continuum robots are composed of arcs that are not perfectly circular, many are approximately so (see e.g. [112, 66, 106]). The remarkable usefulness of the piecewise constant curvature approximation across a wide variety of continuum robot mechanical architectures (discussed in Section 2) combined with its analytical attractiveness has lead to broad application of this modeling approach. Thus, we will focus on piecewise constant curvature kinematics in this paper, before returning in Section 6 to consider the future prospects for both constant and variable curvature modeling and design.

1.1 Contribution

In this paper we contribute a unification of recent kinematic and differential kinematic results for both single-section and multi-section piecewise constant curvature continuum robotics into a common coordinate frame and notational convention, filling in small gaps in the literature where they exist. We demonstrate that several different modeling approaches produce a single, common result for piecewise constant curvature forward kinematics and we clearly delineate the boundaries of robot-specific and robot-independent mappings for both forward and differential kinematics. We also provide a brief historical perspective on continuum robots, discuss some of the basic mechanical designs that have been developed, and provide a perspective on the themes that are shaping future research in continuum robotics.

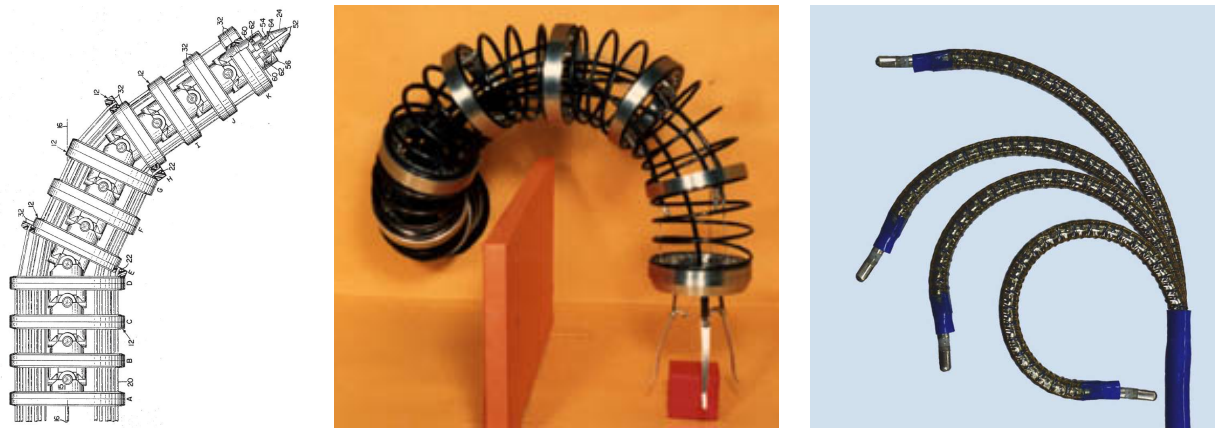

Figure 1: (Left) The Tensor Arm of Anderson and Horn [1] is generally regarded to be the first example of a hyperredundant robot. (Center) The subsequent work of Hirose *et al.* was the first sustained research program in continuum and hyperredundant robots, beginning in the 1970s [37] (image courtesy of Shigeo Hirose). (Right) An example of a modern continuum robot used for medical applications is the Hansen Medical Sensei® system, the kinematics and mechanics of which have been described Camarillo and Salisbury *et al.* [15] (image courtesy of David Camarillo, © [2008] IEEE).

2 Origin, Design, and Applications of Continuum Robots

The origin of continuum robotics is generally traced back to the creation of serpentine robots in the late 1960s [62, pg. 110][79, pg. 110–121]. These hyper-redundant robots employed a number of closely-spaced joints to emulate the motion of the backbone of a snake. Examples include the Orm, which consisted of a series of pneumatically-controlled bellows [67, pg. 68][96], and the tensor arm [1, 2], a tendon-driven robot intended for underseas applications. The weaknesses of the continuum design at that time, which included low payload, poorly-understood kinematics and dynamics, and coarse positioning accuracy, prompted the abandonment in the 1970s of promising research projects that began in the late 1960s [62].

Sustained development of continuum and hyperredundant robots re-emerged in the late 1970s and continued throughout the 1980s and beyond with the pioneering work of Hirose and his team, who developed many novel and innovative designs, paying particular attention to inspiration gleaned from biological systems. Much of this work is summarized in [37]. Industrial continuum manipulators developed during this time period include the Spine robot, a high-dexterity spray-painting robot [57], while other academic efforts included the creation of a trunk-like manipulator [108]. Significant progress in modeling continuum

robots was made in the 1990s, including the introduction of a modal approach [20, 19, 21] establishing a theoretical foundation for continuum robotics based on approximating the shape of a continuum robot using a mathematically tractable curve. Other significant contributions included modeling the underlying continuum mechanics of the robot [46]. In addition, continuum robots continued to be applied in many new and innovative applications in both the commercial [42] and academic research [77] forums.

The first decade of the 21st century has seen a great deal of advancement in the design, modeling, and application of continuum robotics. Much foundational work establishing the theoretical framework for analysis of continuum robotics early in this decade has come from the group of Walker *et al.* [35, 33, 34, 51, 49, 50, 65]. Active areas of current research by many groups include continued advancement in the application of beam theory to create increasingly sophisticated models of continuum robots (see e.g. [33, 15, 106, 81, 30, 98]), and the elucidation of various parsimonious modeling simplifications, including the constant-curvature approximation (e.g. [35, 49, 106]). Many practical applications for continuum and hyperredundant robots have been suggested and/or demonstrated (as shown in Table 1), including undersea manipulation [1, 55], car painting [37, 57], nuclear decontamination [42], nuclear reactor repair [78], waste storage tank remediation [44], liquid transport [24], sanding [44], inspection of unstructured environments and pipes [72, 101, 93, 109, 71, 94], and search and rescue [6, 100].

Continuum robots have also made a significant impact in medicine. A large number of commonly used medical devices such as catheters and colonoscopes can be considered continuum devices. While commonly applied as manually operated instruments, noteworthy efforts have been made to robotize these and other continuum devices for surgery including forceps [64], flexible needles [103], laparoscopic tools [74], endoscopes [40], arthroscopes [27], colonoscopes [75], laser manipulators [36], and catheters [70, 15], among others. Examples of continuum robots developed specifically for surgical applications that do not directly mimic existing surgical devices include the multibackbone throat surgery system of Simaan *et al.* [112], the hyperredundant Cardio Arm of Choset *et al.* [28], and the concentric-tube active

cannula of Webster *et al.* [105, 106, 84, 85, 81] (also developed independently and concurrently by Dupont *et al.* [86, 87, 29, 30]) which is described in Section 3.2.3. In Table 1, "Surgical dexterity" refers to the ability to curve or steer what have traditionally been straight devices such as needles or rigid laparoscopic shafts, enabling them to "turn corners" inside the human body.

Earlier classifications of continuum robots have based their taxonomy on the location of mechanical actuation [77], on backbone architecture, extensibility, and actuation [89], or presented a series of continuum robot prototypes [37]. A review of soft robotics [99] contrasts rigid, hyperredundant, hard continuum, and soft robots and provides a broader overview of biologically-inspired robotics including robotic fish, starfish, trunks, worms, and other creative realizations of soft robots. All of the above are useful ways to categorize continuum and hyperredundant robots, and we draw inspiration from them in compiling Table 1. However, our purpose here is not a comprehensive taxonomy (given the rapidly accelerating recent interest in continuum and hyperredundant robots, such an objective would be perhaps prohibitively challenging), but rather we seek to illustrate the diversity of designs for which the constant curvature forward and differential kinematics we describe in the remainder of this paper are applicable. Here, we omit the subset of hyperredundant robots where constant curvature has not been a primary consideration, either because the robot commonly takes on other shapes, or because the links are long enough that constant curvature is not a useful approximation. This is in no way intended to diminish this very useful class of robot (examples include [38, 72, 20, 31, 92, 110]), and reviews of many of these, particularly those that locomote in a snake-like manner, are available to the interested reader in [37, 97].

Table 1 illustrates the mechanical diversity of continuum robots that approximate piecewise constant curvature. Backbones may be continuous or discrete (hyperredundant robots), and some designs include extensible backbones. Continuum robots consist of multiple serially-linked sections. Each section bends with between one degree of freedom (DOF) (e.g. an inextensible planar robot) and three degrees of freedom (i.e. an extensible robot

Literature	**Classification criteria**								
	Cont./discrete	*Extensible*	*# of sections*	*Actuators/sec.*	*DOF/sec.*	*Actuator spacing*	*Actuation*	*Multi-section coupling*	*Application*
Tensor arm [1, 2]	D		4	4	2	90°	tendon	co-radial	Underwater manipulation
OCRobotics [11, 78]	D		5	3	2	120°	tendon	distributed	Reactor repair
Elephant trunk [35]	D		4	4	2	90°	tendon/spring	co-radial	Bioinspired manipulation
Elephant trunk [24]	C		3	2	2	90°	tendon/spring	co-radial	Liquid transportation
EMMA [9, 44]	D		3	3	2	120°	tendon/spring	co-radial	Sanding, nuclear
Backbone [33]	C		1	1	1	180°	tendon/rod	N/A	General purpose
Tentacle robot [58]	C		2	4	2	90°	tendon/rod	co-radial	General purpose
Arthroscope [27]	D		1	1	2	180°	tendon/rods	N/A	Arthroscopy
Catheter [15, 13]	C	○	2	2	3	90°	tendon/sleeve	distributed	Cardiac surgery
Colobot [18, 16, 17]	C	○	1	3	3	120°	pneumatic	N/A	Colonoscopy
OctArm [49, 50]	C	○	3	3	3	120°	pneumatic	individual	General purpose
Slim Slime 1 [68, 69]	C	○	6	3	3	120°	pneumatic	individual	Search and rescue
Slim Slime 2 [6, 5]	C	○	2	3	3	120°	tendon/pneumatic	co-radial	Search and rescue
Air-OCTOR [50]	C	○	2	3	3	120°	tendon/pneumatic	distributed	General purpose
KSI [42, 43, 41]	C	○	2	3	2	120°	tendon/pneumatic	distributed	Nuclear decontamination
Active catheter [7]	C	○	3	3	2	120°	hydraulic	individual	Cardiac surgery
DDU [89, 112]	C		3	3	2	120°	multibackbone	co-located	Laryngeal surgery
Active cannula [106, 87]	C	○	$2n$	1	2	–	n curved tubes	*	Surgical dexterity
Beveled needle [103]	C	○	∞	0	3	–	tip/tissue	individual	Surgical dexterity

Table 1: A sampling of snake-like robot designs which have been or could be described using constant-curvature kinematics. Intended to be exemplary, not comprehensive. Inspired by the classifications of [89, 37, 77]. *Could be considered co-located or continuously distributed – see Section 3.2.3.

that can bend about two axes without axial rotation). Continuum robots may be under or overactuated, meaning that they can have fewer or more actuators than DOF. An example of a prevalent overactuated design is one whose cables lie at 90° intervals about the central axis (see e.g. [35]). An example of an underactuated robot is a cardiac catheter that uses four wires to actuate two 3-DOF sections [13]. Many different actuation strategies can and have been used, and a few robots are designed to bend only in one plane, to enable enhanced payload capability (see e.g. [38]) or for simplicity of model verification (e.g. the experimental setup in [58]). There have also been a number of approaches to coupling multiple sections together (see the second column from the right in Table 1). On the table, single-section robots are marked N/A, multi-section robots in which each section is mechanically uncoupled from other sections, such as [49], are labeled "individual", and some other options for actuator routing are illustrated in Figure 14, and discussed further in Section 4.

We proceed in subsequent sections of this paper address the kinematic modeling of robots like those on Table 1 that may be approximated as piecewise constant curvature. Section 3 describes constant curvature kinematics, Section 4 addresses multisection forward and inverse kinematics, and Section 5 describes constant curvature differential kinematics.

3 Piecewise Constant Curvature Kinematics

Constant curvature has often been viewed as a desirable characteristic in continuum robots due to the simplifications it enables in kinematic modeling. Variable curvature elastic structures [54] are described by functions that are integrated, whereas constant curvature robots can be considered as consisting of a finite number of curved links. These links are described by a finite set of arc parameters, which can be converted to analytical frame transformations, as will be discussed in this section. Thus, constant curvature can facilitate additional analysis on topics such as differential kinematics, real-time control, and other useful computations.

The constant-curvature assumption has been successfully applied to many continuum robots. For example, if a constant moment is applied along a beam, Bernoulli-Euler beam

mechanics predicts a constant curvature result [33]. This is the case for the initial simple models derived for the active cannula design described in Section 3.2.3, in which concentric precurved tubes (under the torsionless assumption) directly apply constant moments to one another. Arguments in [58] demonstrate that a constant moment can be applied by a cable terminating at the end of a flexible rod and passing through a sufficient number of cable guides fixed along the rod (see Section 3.2.2). Likewise, the pneumatically-actuated trunks described in Section 3.2.1 can be considered piecewise constant curvature because the actuators closely approximate the application of a moment to the end of the trunk [49]. Many other continuum robots have also been observed to exhibit approximate constant curvature (e.g. [35, 89, 1, 37, 24, 42], among others).

The piecewise constant curvature assumption has the advantage of enabling kinematics to be decomposed into two mappings [49], as visualized in Figure 2. One is from joint or actuator space, $\boldsymbol{q}$, to configuration space parameters that describe constant-curvature arcs. The other is from this configuration space to task space, consisting of a space curve which describes position and orientation along the backbone. Examples of actuator variables include lengths of cables, flexible push rods, or pneumatic tubes. Arc parameters, which define the configuration space of the robot, consist of triplets of curvature ($\kappa(\boldsymbol{q})$), the angle of the plane containing the arc ($\phi(\boldsymbol{q})$), and arc length ($\ell(\boldsymbol{q})$, or sometimes $s \in [0 \quad \ell]$), as shown in Figure 3(b). Alternatively, the relationship $\theta = \kappa s$ allows parameterization based on the angle θ through which the arc bends (see e.g. [90]).

The mapping $\boldsymbol{f}_{specific}$ from actuator space $\boldsymbol{q}$ to the configuration space of arc parameters $(\boldsymbol{\kappa}, \boldsymbol{\phi}, \boldsymbol{\ell})$ is robot-specific, since actuators in each unique robot design influence arc parameters in different ways. In particular, consideration of the forces and moments applied by actuators coupled with suitable approximations (e.g. the application of a constant moment as discussed earlier) yields this mapping from actuator variables (pressure, length, etc.) to circular sections described by arc parameters in configuration space. In contrast, the mapping $\boldsymbol{f}_{independent}$ from arc parameters to pose $\boldsymbol{x}$ along the backbone is robot-independent because it is applicable to all systems that can be approximated as piecewise constant cur-

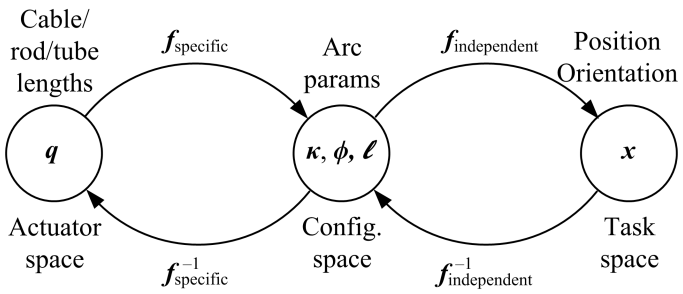

Figure 2: The three spaces and mappings between them which define the kinematics of constant-curvature robots. A robot-specific mapping, discussed in Section 3.2, transforms actuator space variables $\boldsymbol{q}$ to configuration space variables $(\boldsymbol{\kappa}, \boldsymbol{\phi}, \boldsymbol{\ell})$. Next, a robot-independent mapping takes these configuration space variables to the task space, as developed in the following section. Section 4.2 reviews inverse mappings for both the robot-specific and the robot-independent cases.

vature arcs. This is a purely kinematic mapping, transforming from arc parameters to a space curve in task space. In the following sections, we first describe methods of accomplishing the robot-independent mapping, then proceed to consider several case studies on the robot-specific mapping for robots with varying types of actuators.

3.1 The Robot-Independent Mapping

A wide variety of conventions, formalisms, and coordinate frame choices exist in the literature to accomplish forward kinematics. In this section, we show that the various methods all fundamentally produce the same result for piecewise constant curvature robots. To illustrate this, we choose a frame convention and use it throughout the paper, recasting results from the literature using this convention, which Figure 3 illustrates. Specifically, we consider the $+z$ axis to be tangent to the base of the continuum robot. When $\phi = 0$, positive curvature $(\kappa > 0)$ produces bending about the $+y$ axis such that when the continuum robot backbone has traced out an angle of π radians it will touch the $+x$ axis. Below, we describe several different approaches to derive the position and orientation of the centerline of the robot.

Referring to Figure 2, this section therefore defines $\boldsymbol{f}_{independent}$ in terms of the homogeneous transformation matrix T parameterized by $(\boldsymbol{\kappa}, \boldsymbol{\phi}, \boldsymbol{\ell})$. This matrix gives task space coordinates $\boldsymbol{x} = \mathrm{T}_{1\ldots3,4}$. This section begins development of this mapping with a geometric argument.

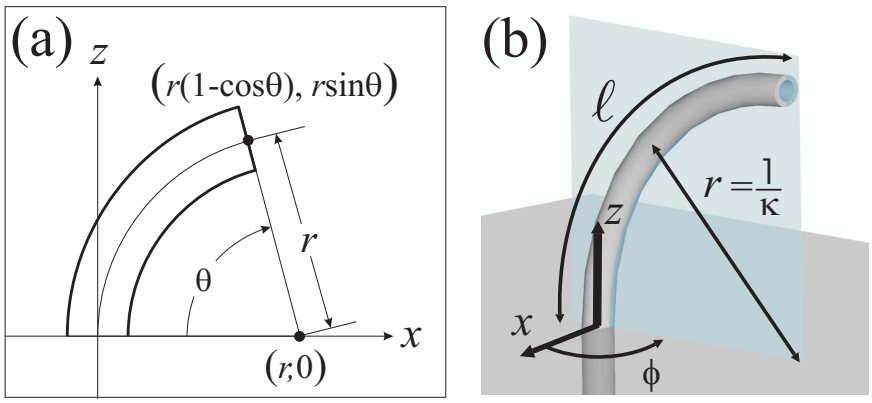

Figure 3: (a) When ϕ is zero, the arc lies in the $x-z$ plane as shown. (b) The angle ϕ rotates the arc out of the $x-z$ plane. This figure shows the "arc parameters" that describe a circular arc, namely curvature (κ), plane (ϕ), and arc length (ℓ). The axes shown in both figures are those of the fixed spatial frame.

3.1.1 Arc Geometry

The geometry of a continuum robot provides a means of determining the pose of points along it [102, 66, 35, 7]. In Figure 3(a), when $\phi = 0$ the coordinates of a point on the circular arc of radius r in the $x-z$ plane centered at $\begin{bmatrix} r & 0 & 0 \end{bmatrix}^{\mathrm{T}}$ are $\boldsymbol{p} = \begin{bmatrix} r(1-\cos\theta) & 0 & r\sin\theta \end{bmatrix}^{\mathrm{T}}$. Note also that this motion includes a rotation $\mathrm{R}_y(\theta)$ about the $+y$ axis, where $R_y(\theta) \in \mathrm{SO}(3)$ indicates a rotation about the y axis by the angle θ. Rotating the entire arc about the $+z$ axis by ϕ moves the robot out of the $x-z$ plane, producing a transformation from arc base to tip,

$$\mathrm{T} = \underbrace{\begin{bmatrix} \mathrm{R}_z(\phi) & 0 \\ 0 & 1 \end{bmatrix}}_{\text{Rotation}} \underbrace{\begin{bmatrix} \mathrm{R}_y(\theta) & \boldsymbol{p} \\ 0 & 1 \end{bmatrix}}_{\text{Inplane Transformation}}. \tag{1}$$

Noting that $\kappa = 1/r$ and $\theta = \kappa s$ (where $s \in [0 \quad \ell]$), this can be written in terms of "arc parameters" (κ, ϕ, ℓ) as follows. Here, to emphasize that this transformation can be written at any point s along the arc from 0 to ℓ we use the s symbol and write,

$$\boldsymbol{f}_{independent} = \mathrm{T} = \begin{bmatrix} \cos\phi\cos\kappa s & -\sin\phi & \cos\phi\sin\kappa s & \frac{\cos\phi(1-\cos\kappa s)}{\kappa} \\ \sin\phi\cos\kappa s & \cos\phi & \sin\phi\sin\kappa s & \frac{\sin\phi(1-\cos\kappa s)}{\kappa} \\ -\sin\kappa s & 0 & \cos\kappa s & \frac{\sin\kappa s}{\kappa} \\ 0 & 0 & 0 & 1 \end{bmatrix}. \tag{2}$$

Note that the tip frame in (1) and (2) is aligned so that the x axis points toward the center of the circle. In some applications (e.g. when a gripper is attached to the tip of the arc), it may be useful to orient the tip frame such that it aligns with the base frame when "slid" along the arc to the base without rotation about the local z axis (that is, use of a Bishop's frame [8]). This can be obtained by post multiplying T by a homogeneous transformation with rotation $\mathrm{R}_z(-\phi)$ and translation $\mathbf{0}$, yielding an alternate $\boldsymbol{f}_{independent}$ of

$$\mathrm{T}_{\mathrm{w}} = \begin{bmatrix} \cos^2\phi(\cos\kappa s - 1) + 1 & \sin\phi\cos\phi(\cos\kappa s - 1) & \cos\phi\sin\kappa s & \frac{\cos\phi(1-\cos\kappa s)}{\kappa} \\ \sin\phi\cos\phi(\cos\kappa s - 1) & \cos^2\phi(1-\cos\kappa s) + \cos\kappa s & \sin\phi\sin\kappa s & \frac{\sin\phi(1-\cos\kappa s)}{\kappa} \\ -\cos\phi\sin\kappa s & -\sin\phi\sin\kappa s & \cos\kappa s & \frac{\sin\kappa s}{\kappa} \\ 0 & 0 & 0 & 1 \end{bmatrix}. \tag{3}$$

As we review in the remainder of this section, these results can and have been derived in a variety of ways, including via Denavit-Hartenburg parameters [35], Frenet-Serret frames [35], a similar integral formulation that can account for zero curvature [20] (the Frenet-Serret frame is undefined when curvature equals zero), and exponential coordinates [103, 106, 86]. Our review highlights the fact that while derivations in the literature may appear different at first glance due to the diversity of frame choices, formalisms, and symbols employed, they arrive at the same final result when piecewise constant curvature is assumed.

3.1.2 Denavit-Hartenburg Parameters

Forward kinematics for a segment of a piecewise constant curvature robot as given in (2) and (3) can be derived using the Denavit-Hartenburg method, augmented with transformations between D-H parameters and arc parameters (ϕ, κ, ℓ). In this subsection, ϑ_i variables describe

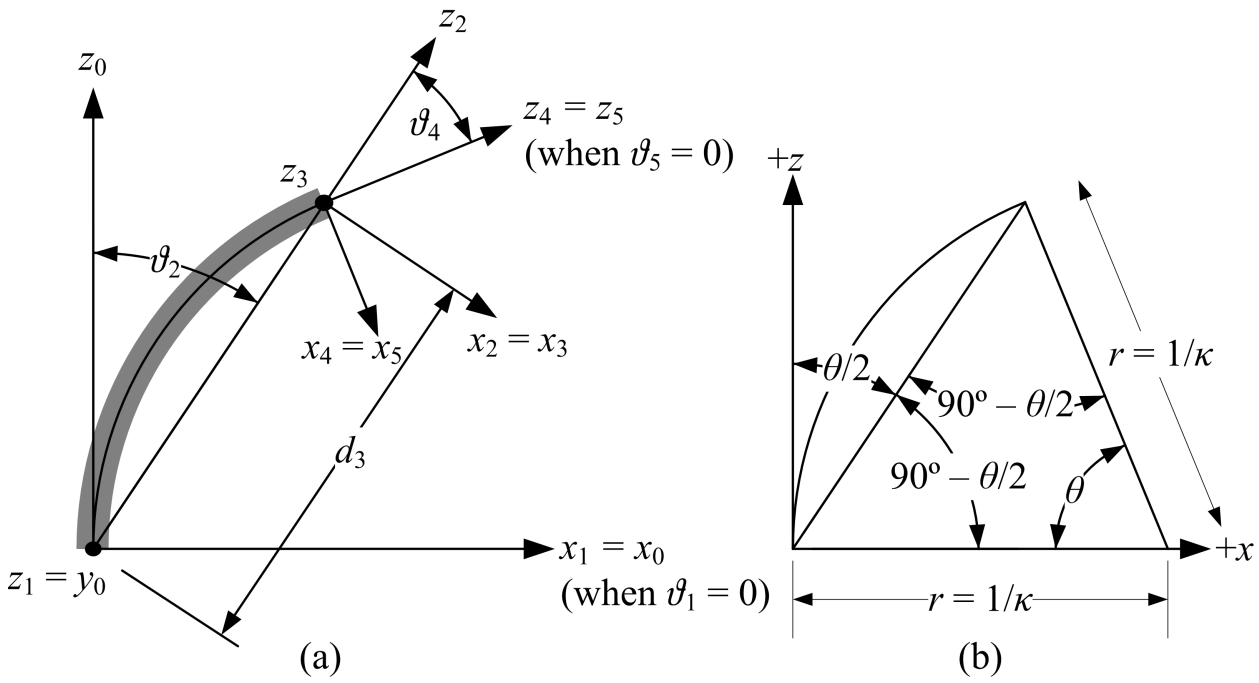

Figure 4: (a) D-H axes used to construct a rigid-link backbone for a continuum robot. The resulting D-H table is given in Table 2. All vectors remain in the plane, except for z_1 and z_3 which extend out of the paper and are therefore diagrammed as dots. (b) Given an arc which cuts through θ degrees extending from the origin tangent to the $+z$ axis and bending about the $+y$ axis, per the conventions established in this paper, the angle between the z axis and a line connecting the origin to the arc tip is $\theta/2$.

rotations about the local z axis, not to be confused with the separate use of θ to define the angle through which the arc bends as shown in Figure 3(a). One D-H table and mapping, given in [49], models a single curved arc as consisting of a first pair and final pair of ball-and-socket joints. Another approach introduced in [35] decomposes the problem, in a manner similar to the geometric argument above, as an inplane transformation together with a rotation of the arc about the z axis by $\vartheta_1 = \phi$.

Following this second approach, the inplane transformation (whose D-H parameters are given in links 2-4 of Table 2) is illustrated in Figure 4(a). This is constructed by first rotating about z_1 by ϑ_2 to point z_2 toward the continuum robot's tip, then translating by d_3 along z_2 to move to the robot's tip, and finally rotating about z_3 by ϑ_4 to align z_4 with the backbone tangent direction. As discussed in the previous section, an optional final rotation of ϑ_5 about z_4 provides an alternate choice of end-effector frame orientation. Note that the

Link	ϑ	d	a	α
1	$\vartheta_1 = \phi$	0	0	$-\pi/2$
2	$\vartheta_2 = \kappa s/2$	0	0	$\pi/2$
3	0	$d_3 = (2/\kappa)\sin\kappa s/2$	0	$-\pi/2$
4	$\vartheta_4 = \kappa s/2$	0	0	$\pi/2$
5	$\vartheta_5 = -\phi$	0	0	0

Table 2: DH parameter table for a single section of a piecewise constant curvature continuum robot, as given in Figure 4. In the above table "link" refers to the several imaginary robot links used to model a single section of a continuum robot. Mappings from D-H to arc parameters derived in the text are included.

entries in Table 2 have been modified from [35] so that the arc curves about the y axis, following the convention established earlier.

The relationships between D-H parameters and arc parameters are given in Table 2. Insight on these relationships can be obtained by observing that Figure 4 shows $\vartheta_2 = \vartheta_4 = \theta/2$ and $\vartheta_1 = \phi$. Tip coordinates in 2-D, given in Figure 3(a), yield $d_3 = r\sqrt{2(1-\cos\theta)} = 2r\sin\theta/2$ (since $1-\cos\theta = 2\sin^2\theta/2$). The relationships $\theta = \kappa s$ and $\kappa = 1/r$ complete the mapping. With these relationships, the D-H table corresponds to the transformation given in (2). Including the optional ϑ_5 yields (3).

3.1.3 Frenet-Serret Frames

Differential calculus provides a rich set of tools for describing the evolution of a curve in space, forming the basis for describing the static and dynamic behavior of nonlinearly elastic rods [4]. In particular, use of the the Frenet-Serret formulas provide a third means of deriving the forward kinematics of piecewise circular robots. Reviewing [35], the Frenet-Serret equations parameterize a curve in terms of arc length s by defining a local coordinate frame shown in Figure 5 which moves along the curve in terms of a unit vector tangent to the curve $\boldsymbol{t}(s)$, a unit vector $\boldsymbol{n}(s)$ which is normal to the curve, and a unit binormal vector $\boldsymbol{b}(s) = \boldsymbol{t}(s) \times \boldsymbol{n}(s)$ perpendicular to both the tangent and normal vectors. Two functions, the curvature $\kappa(s)$

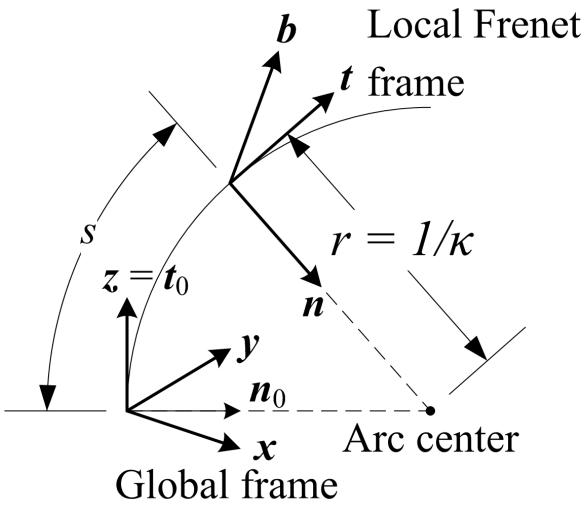

Figure 5: An illustration of the Frenet-Serret coordinate frame used to describe a constant-curvature continuum robot. This local coordinate frame consists of a vector $\boldsymbol{t}$ tangent to the curve, a vector $\boldsymbol{n}$ normal to the curve, and a binormal vector $\boldsymbol{b}$ to complete the frame. The constant curvature κ defines the radius of the resulting arc, while the initial condition $\boldsymbol{n}_0$ defines the angle of the plane containing the arc. The choice of $\boldsymbol{t}_0$ to lie along the $+z$ axis causes the curve to extend along that axis, per convention.

and torsion $\tau(s)$, determine the evolution of the curve as

$$\begin{aligned}
\boldsymbol{t}'(s) &= \kappa(s)\boldsymbol{n}(s) \\
\boldsymbol{n}'(s) &= -\kappa(s)\boldsymbol{t}(s) + \tau(s)\boldsymbol{b}(s) \\
\boldsymbol{b}'(s) &= -\tau(s)\boldsymbol{n}(s),
\end{aligned}$$

where the prime indicates differentiation with respect to s. Noting that many continuum robots are constructed to reduce torsion where possible, and recalling the constant-curvature assumption, $\kappa(s) \equiv \kappa$ and $\tau(s) \equiv 0$. The defining equations of a continuum robot are therefore $\boldsymbol{t}'(s) - \kappa\boldsymbol{n}(s) = 0$ and $\boldsymbol{n}'(s) = -\kappa\boldsymbol{t}(s)$. Differentiating and substituting, $\boldsymbol{t}''(s) + \kappa^2\boldsymbol{t}(s) = 0$. Solving,

$$\boldsymbol{t}(s) = \boldsymbol{t}_0 \cos\kappa s + \boldsymbol{n}_0 \sin\kappa s, \tag{4}$$

where $\boldsymbol{t}_0 = \boldsymbol{t}(0)$ and $\boldsymbol{n}_0 = \boldsymbol{n}(0)$.

To obtain coordinates along the curve $\boldsymbol{p}(\ell)$, it is possible to integrate the tangent vector

$$\boldsymbol{p}(\ell) = \int_0^\ell \boldsymbol{t}(s)\, ds = \boldsymbol{t}_0 \kappa^{-1} \sin \kappa\ell + \boldsymbol{n}_0 \kappa^{-1}(1 - \cos \kappa\ell). \tag{5}$$

Derivation of the above result for the planar case can be found in [35], and it can be extended to 3D as follows. According to the convention established in the previous section, the $+z$ axis is tangent to the continuum robot at its base, making the initial tangent vector $\boldsymbol{t}_0 = \begin{bmatrix} 0 & 0 & 1 \end{bmatrix}^{\mathrm{T}}$. The initial normal vector is perpendicular to $\boldsymbol{t}_0$ and depends on the direction of curvature defined by the angle ϕ, so that $\boldsymbol{n}_0 = \begin{bmatrix} \cos\phi & \sin\phi & 0 \end{bmatrix}^{\mathrm{T}}$. Substituting these initial conditions into (4),

$$\boldsymbol{t}(s) = \begin{bmatrix} \cos\phi \sin\kappa s & \sin\phi \sin\kappa s & \cos\kappa s \end{bmatrix}^{\mathrm{T}}. \tag{6}$$

Integrating $\boldsymbol{p}$ in (5) under these initial conditions produces a tip position identical to $\boldsymbol{p}$ in (2).

The local coordinate frame vectors $\boldsymbol{t}$, $\boldsymbol{n}$, and $\boldsymbol{b}$ provide orientation for the tip frame. First, note that the choice of an initial tangent vector $\boldsymbol{t}_0$ maps $\boldsymbol{t}$ in the base frame to the $+z$ axis. Likewise, the initial normal vector $\boldsymbol{n}_0$ points toward the center of the arc, agreeing with the frame convention established in Section 3.1.1, implying that the orientation is $\mathrm{R} = \begin{bmatrix} \boldsymbol{n} & \boldsymbol{b} & \boldsymbol{t} \end{bmatrix}$. Substituting (6) into the relationship $\boldsymbol{n}'(s) = -\kappa \boldsymbol{t}(s)$, $\boldsymbol{n}(s) = -\kappa \int \begin{bmatrix} \cos\phi \sin\kappa s & \sin\phi \sin\kappa s & \cos\kappa s \end{bmatrix}^{\mathrm{T}} ds$ yielding $\boldsymbol{n}(s) = \begin{bmatrix} \cos\phi \cos\kappa s & \sin\phi \cos\kappa s & -\sin\kappa s \end{bmatrix}^{\mathrm{T}}$ and $\boldsymbol{b}(s) = \boldsymbol{t}(s) \times \boldsymbol{n}(s) = \begin{bmatrix} -\sin\phi & \cos\phi & 0 \end{bmatrix}^{\mathrm{T}}$. Assembling these columns gives the rotational portion of the matrix in (2).

3.1.4 Integral Representation

While differential curve representations other than Frenet-Serret are possible (see e.g. [8]), another approach given in [20] is the integral representation of a curve, also used in the dynamics formulation of [45]. This integral formulation avoids difficulties which arise in the Frenet-Serret (F-S) formulas when $\kappa = 0$ and avoids the necessity of solving a differential

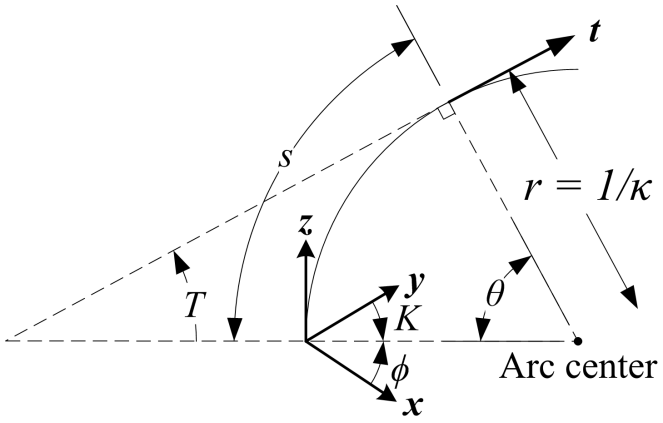

Figure 6: The integral representation defines the tangent vector $\boldsymbol{t}$ (given in (7)) to the arc in terms of one function ($K(s)$) which gives the angle in the xy plane measured clockwise from the $+y$ axis, and another ($T(s)$) which specifies the elevation. The connection to the arc parameters (κ,ϕ,ℓ) used throughout this paper can be made by observing that based on the geometry above $K = \pi/2 - \phi$ and $T = \pi/2 - \theta$, where $\theta = \kappa s$.

equation to extract the curve, given arc length parameterized curvature and torsion functions.

Like the Frenet-Serret approach, integration of a vector $\boldsymbol{t}(s)$ tangent to the curve at s determines the shape of the curve, where

$$\boldsymbol{t}(s) = \begin{bmatrix} l(s)\sin K(s)\cos T(s) \\ l(s)\cos K(s)\cos T(s) \\ l(s)\sin T(s)ds \end{bmatrix}. \tag{7}$$

In this equation, $l(s)$ specifies dilation, where $l = 1$ produces a curve that is neither compressed (when $l < 1$) or extended ($l > 1$). The angle $K(s)$ gives the orientation of the tangent vector $\boldsymbol{t}$ in the xy plane, measured clockwise from the y axis, and $T(s)$ gives the angle between $\boldsymbol{t}$ and the xy plane, as shown in Figure 6. From [20], tip position is defined as

$$\boldsymbol{p}(\ell) = \int_0^\ell \boldsymbol{t}(s)ds. \tag{8}$$

Applying this formulation to the constant-curvature inextensible case implies that $l(s) \equiv 1$.

Referring again to Figure 6 or equivalently setting (7) equal to (6), the angles

$$\begin{aligned} K(s) &= \pi/2 - \phi \\ T(s) &= \pi/2 - \kappa s \end{aligned} \tag{9}$$

define a vector $\boldsymbol{t}$ tangent to a constant-curvature arc using the frame convention chosen for this paper. With these definitions, integrating (8) produces a tip position identical to $\boldsymbol{p}$ in (2) and (3).

With respect to orientation, [20] defines an "induced" reference frame along the backbone, which differs from the F-S frame by a rotation about the tangent vector. To see how this representation agrees with (2) for the constant curvature case, one must simply relabel axes ([20] has the $\boldsymbol{e}_2$ or y axis of the local frame tangent to the curve) such that the frame remains right handed, with $\boldsymbol{e}_3$ (or z) tangent to the curve. This results in a shuffling of the columns of the induced rotation matrix Q_{IR} provided in [20]. Then, substituting (9) into the resulting Q_{IR} yields the rotation matrix given in (2).

3.1.5 Exponential Coordinates

Similar results can be obtained using exponential coordinates based on Lie Group theory [103, 106, 86]. See also [63] for a thorough treatment of exponential coordinates – in this section we follow the notation and conventions outlined therein. Recalling from (1) that the homogeneous transformation for a circular arc can be decomposed into a rotation and an inplane transformation, we can write the twist coordinates associated with each as

$$\boldsymbol{\xi}_{rot} = \begin{bmatrix} \boldsymbol{v}_{rot} \\ \boldsymbol{\omega}_{rot} \end{bmatrix} = \begin{bmatrix} 0 & 0 & 0 & 0 & 0 & 1 \end{bmatrix}^{\mathrm{T}} \quad \text{and} \tag{10}$$

$$\boldsymbol{\xi}_{inp} = \begin{bmatrix} \boldsymbol{v}_{inp} \\ \boldsymbol{\omega}_{inp} \end{bmatrix} = \begin{bmatrix} 0 & 0 & 1 & 0 & \kappa & 0 \end{bmatrix}^{\mathrm{T}}, \tag{11}$$

respectively, where $\boldsymbol{v}$ and $\boldsymbol{\omega}$ are linear and angular differential motions. Then, writing the twist coordinates as twists,

$$\widehat{\boldsymbol{\xi}}_{rot} = \begin{bmatrix} \widehat{\boldsymbol{\omega}}_{rot} & \boldsymbol{v}_{rot} \\ 0 & 0 \end{bmatrix} = \begin{bmatrix} 0 & -1 & 0 & 0 \\ 1 & 0 & 0 & 0 \\ 0 & 0 & 0 & 0 \\ 0 & 0 & 0 & 0 \end{bmatrix} \text{ and } \widehat{\boldsymbol{\xi}}_{inp} = \begin{bmatrix} \widehat{\boldsymbol{\omega}}_{inp} & \boldsymbol{v}_{inp} \\ 0 & 0 \end{bmatrix} = \begin{bmatrix} 0 & 0 & \kappa & 0 \\ 0 & 0 & 0 & 0 \\ -\kappa & 0 & 0 & 1 \\ 0 & 0 & 0 & 0 \end{bmatrix}^{\mathrm{T}}, \quad (12)$$

where as shown, $\widehat{\ }$ maps from $\mathbb{R}^3$ to $\mathfrak{so}(3)$ (the Lie algebra of SO(3)) and also $\mathbb{R}^6$ to $\mathfrak{se}(3)$ (the Lie algebra of SE(3)), as used in [63]. Applying the product of exponentials formula yields

$$\mathrm{T} = e^{\left(\widehat{\boldsymbol{\xi}}_{rot}\phi\right)} e^{\left(\widehat{\boldsymbol{\xi}}_{inp}\ell\right)}, \quad (13)$$

which is identical to (1) and evaluates to (2). Similarly, the single set of twist coordinates

$$\boldsymbol{\xi} = \begin{bmatrix} 0 & 0 & 1 & -\kappa\sin\phi & \kappa\cos\phi & 0 \end{bmatrix}^{\mathrm{T}} \quad (14)$$

exponentiated as $e^{\left(\widehat{\boldsymbol{\xi}}\ell\right)}$ yields (3).

3.1.6 Summary of Robot-Independent Mapping

In summary, we have shown in this section that the derivation of a robot-independent mapping for the forward kinematics of a piecewise constant curvature robot can be accomplished with a variety of approaches. Our primary purpose here was to show that many seemingly disparate approaches produce identical results (namely (2) and (3) when written in homogeneous matrix form) when placed in a common coordinate frame and stated using consistent symbols and mathematical terminology. While this may be clear to researchers experienced in the field, it is our experience that for newcomers to continuum robotics, arriving at this conclusion requires significant effort and an intensive literature survey, which has led to some results being redemonstrated multiple times in the literature. It is our hope that this exposition will provide an easier entry into continuum robotics for new researchers, and also

illustrate the diversity of approaches available to those pursuing extensions to basic constant curvature theory, as discussed in Section 6.

3.2 Robot-Specific Arc Parameter Mappings

The robot-independent mapping $\boldsymbol{f}_{independent}$ (see Figure 2) developed thus far results from the solution of a purely kinematic problem, namely that of mapping a piecewise constant curvature arc described in configuration space $(\boldsymbol{\kappa}, \boldsymbol{\phi}, \boldsymbol{\ell})$ to a task space position and orientation ($\boldsymbol{x}$, which can be expressed as a homogeneous transformation matrix). In contrast, the robot-specific mapping $\boldsymbol{f}_{specific}$ maps from actuator or joint space (e.g. tendon lengths, pneumatic chamber pressures, etc.) to configuration space $(\boldsymbol{\kappa}, \boldsymbol{\phi}, \boldsymbol{\ell})$. This mapping is usually developed by examining the forces and moments applied by the actuators and transmitted through the structure of a continuum robot. Sometimes simplifying assumptions are introduced in this analysis, the most common being that constant moments are applied along the robot, implying (by Bernoulli-Euler beam mechanics) that it will assume a circular arc.

Because the manner in which actuators define arc parameters is generally unique to each actuation strategy, developing this mapping requires modeling of actuator-support structure interaction. In this section we provide several case studies for how the robot-specific mapping has been obtained for continuum robots with different actuation methods. Herein, we provide references to original source material, then present results (simplified where possible, and cast in the notation of this paper) for several common continuum robot designs, which cover most of the actuation strategies currently in use.

3.2.1 Robots Shaped by Continuously Bending Actuators

One common style of continuum robot construction (e.g. [18, 50, 69, 7] among others) is composed of actuators which bend continuously, such as flexible rods or pneumatic tubes. Figure 7 shows two realizations of such designs. A closed-form relationship between actuator lengths and the resulting shape is useful for real-time control which enables applications such as those discussed in Section 2.

Therefore, we seek to derive expressions for the arc parameters $(\ell(\boldsymbol{q}), \kappa(\boldsymbol{q}), \phi(\boldsymbol{q}))$ for a single-section, 3-actuator continuum robot, as a function $\boldsymbol{f}_{specific}$ (see Figure 2) of the "joint variables" $\boldsymbol{q} = \begin{bmatrix} l_1 & l_2 & l_3 \end{bmatrix}^{\mathrm{T}}$ which describe the lengths of three pneumatic chambers or three flexible rods. What follows is a simplified version of derivations which can be found in [7, 16], and [112] provides an equivalent approach using a two-angle parametrization rather than the angle-curvature approach presented in this paper.

Figure 8(a) provides a view of the base and top of a single-section continuum robot, while Figure 8(b) shows the base of the same section viewed from above while looking down along the z axis. As shown by the geometry in the figure, the radius of curvature r measured from the robot's center relates to the radius of curvature for each individual actuator (denoted by $i \in 1 \ldots 3$) according to

$$r_i = r - d\cos\phi_i, \tag{15}$$

where d is the distance from the center of a section of the robot to the center of the actuator (which is the same for all actuators) and ϕ_i specifies the angle between the robot's bending direction and the location of actuator i.

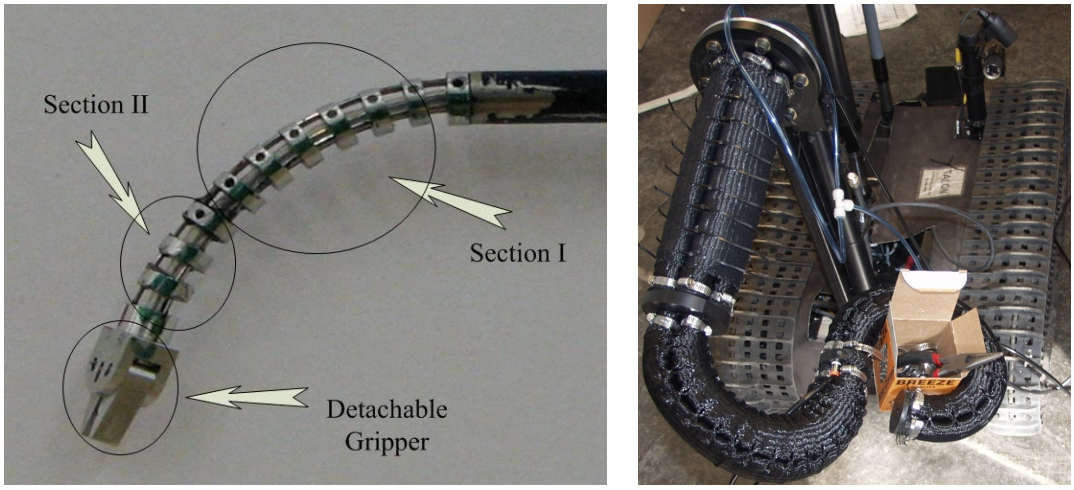

Figure 7: Examples of flexible push-rod (left) and pneumatic (right) continuum robots with three actuators spaced at 120° radial intervals, whose kinematics are derived in Section 3.2.1. The 4.2 mm diameter multi-backbone robot by Simaan *et al.* [111] is designed for teleoperated surgery in the throat and airways. The OctArm robot [49] is mounted on a tracked, mobile base and actuated by latex rubber tubes, which are covered by a mesh which produces extension when pressurized. Left photo courtesy of Nabil Simaan, © [2006] IEEE. Right photo courtesy of Chris Rahn, © [2006] IEEE.

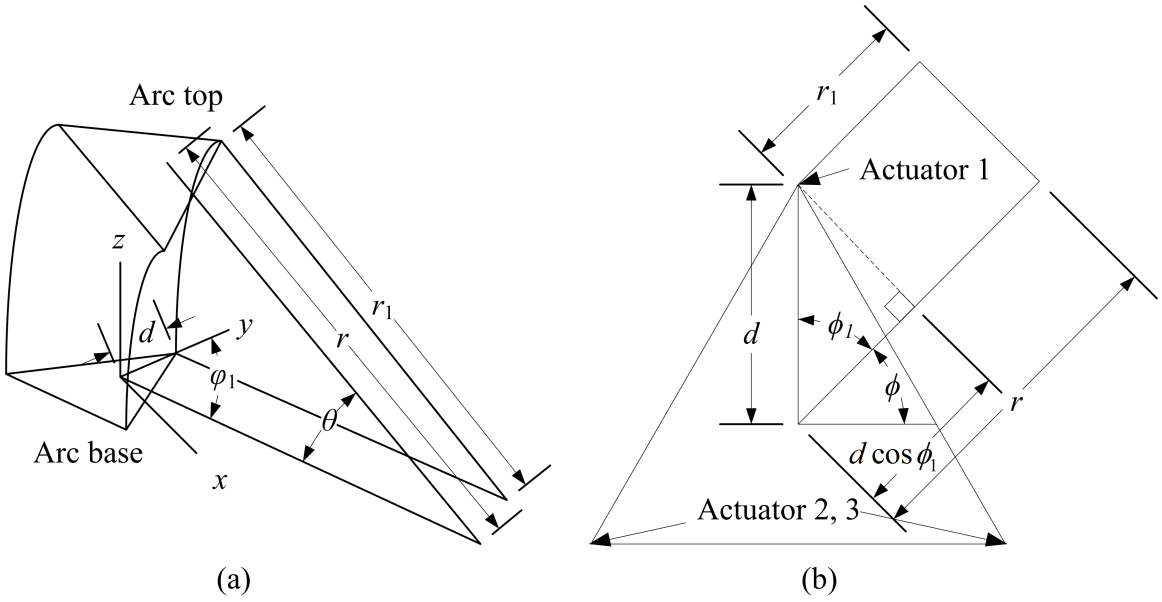

Figure 8: (a) An illustration of an arc section in which various arc parameters are defined. (b) A diagram of the base section seen from above, from which (15) results.

Multiplying (15) by the arc angle θ illustrated in Figure 8(b) and recalling that $\ell = \theta r$ and $l_i = \theta r_i$, the relationship between the arc length of the robot (ℓ) and the arc length of the i^{th} actuator (l_i) is

$$\ell = l_i + \theta d \cos\phi_i. \tag{16}$$

Given this relationship, it is possible to determine $\ell(\boldsymbol{q})$ by noting that actuator locations (as shown in Figure 8) are related to the bending plane of the robot $\phi(\boldsymbol{q})$ by $\phi_1 = 90° - \phi$, $\phi_2 = 210° - \phi$, and $\phi_3 = 330° - \phi$. Therefore, $\sum_{i=1}^{3} \cos\phi_i = 0$. Thus, combining (16) from $i = 1 \ldots 3$ yields

$$\ell(\boldsymbol{q}) = \frac{l_1 + l_2 + l_3}{3}. \tag{17}$$

Equation (16) determines $\phi(\boldsymbol{q})$ as follows. Applying (16) to the first two actuators and setting the right hand sides equal yields $\theta d = (l_2 - l_1)/(\cos\phi_1 - \cos\phi_2)$. To obtain ϕ, apply the same procedure to actuators 2 and 3, equate the results, and insert the above-mentioned relationships between ϕ_i and ϕ to obtain

$$\phi(\boldsymbol{q}) = \tan^{-1}\left(\frac{\sqrt{3}\,(l_2 + l_3 - 2l_1)}{3\,(l_2 - l_3)}\right). \tag{18}$$

To obtain the curvature of the robot $\kappa(\boldsymbol{q})$, first recall that $\theta = \kappa\ell = l_i/r_i$, so that $r_i = l_i/\kappa\ell$, which when combined with (15) yields $\kappa = (\ell - l_i)/\ell d\cos\phi_i$. Considering a single actuator (e.g. $i = 1$ so that $\phi_1 = 90^\circ - \phi$) in (17) implies that $\kappa = (l_2 + l_3 - 2l_1)/\left((l_1 + l_2 + l_3)\, d \sin\phi\right)$. Combining this and (18) with the identity $\sin\left(\tan^{-1}(y/x)\right) = y/\sqrt{x^2 + y^2}$ and simplifying yields the desired result, namely,

$$\kappa(\boldsymbol{q}) = \frac{2\sqrt{l_1^2 + l_2^2 + l_3^2 - l_1 l_2 - l_1 l_3 - l_2 l_3}}{d(l_1 + l_2 + l_3)}. \tag{19}$$

In summary, equations (17-19) give the robot-specific map $\boldsymbol{f}_{specific}$ from actuators to arc parameters $(\ell(\boldsymbol{q}), \kappa(\boldsymbol{q}), \phi(\boldsymbol{q}))$. The shape of the robot's section can then be obtained via the results given in Section 3.1. This framework also applies to multisection robots; each section can be independently considered and will yield one set of arc parameters.

The kinematics for the 4-actuator case can be considered in a similar manner to the 3-actuator derivation above, although it has not specifically been articulated in this way in the literature as far as the authors are aware. For continuum robots with four actuators, $\phi_1 = \cos\phi$, $\phi_2 = \cos(90^\circ - \phi) = \sin\phi$, $\phi_3 = \cos(180^\circ - \phi) = -\cos\phi$, and $\phi_4 = \cos(270^\circ - \phi) = -\sin\phi$. Following the same steps as the 3-actuator derivation above yields the desired result. Specifically, combining (16) from $i = 1 \ldots 4$ yields

$$\ell(\boldsymbol{q}) = \frac{l_1 + l_2 + l_3 + l_4}{4}. \tag{20}$$

Applying (16) to actuators 1 and 3 then to 2 and 4, equating θd, then solving gives

$$\phi(\boldsymbol{q}) = \tan^{-1}\left(\frac{l_4 - l_2}{l_3 - l_1}\right). \tag{21}$$

Finally, choosing actuator 2 and recalling $\kappa = (\ell - l_i)/\ell d\cos\phi_i$, substituting (20) and (21) produces

$$\kappa(\boldsymbol{q}) = \frac{(l_1 - 3l_2 + l_3 + l_4)\sqrt{(l_4 - l_2)^2 + (l_3 - l_1)^2}}{d\,(l_1 + l_2 + l_3 + l_4)\,(l_4 - l_2)}, \tag{22}$$

which completes the derivation.

However, before we leave this topic, a few words are in order regarding the mechanical arrangement of some robots, particularly those actuated by push rods [111] that are over-actuated. Here, an additional inextensible central rod defines a constant length ℓ of each section of the robot. In this case, (17) shows that knowledge of two rod lengths l_1, l_2 defines the required length l_3 for the third rod, assuming all three rods bend with constant curvature. This kinematic over-determination is valuable – one can choose a redundancy resolution that minimizes the load on each backbone and thus reduces the risk of buckling [88]. We also note that for wire-actuated robots, which may be either under- or over-actuated, additional complexities arise in constructing multisection robots, due to coupling between cables which pass through multiple sections. The multisection case is discussed in Section 4.

3.2.2 Robots Shaped by Tendons

A second frequently applied continuum robot design (e.g. [35, 24, 50, 42]) utilizes three cables, as shown in Figure 9. Cable guides placed at equally-spaced intervals along the robot cause its shape to approximate a circular arc, while dividing the cables into line segments which inscribe the arc formed by the robot. Measuring and controlling cable length then enables shape description and control based on the analytical relationships developed below.

One derivation for the forward kinematics of a single-section 3-cable cable-driven continuum robot was provided in [49]. Here we contribute a simplified derivation, which is similar to the one described in the previous section for robots shaped by continuously bending actuators. As in the previous section, this procedure can then be repeated to derive 4-cable kinematics. Here, we assume cables travel in a straight line from one cable guide to the next in a uniformly-bending section of the robot, subdividing each section into n units that begin and end at the $n+1$ cable guides as shown in Figure 10. Examining one unit of an n–unit section, note that equation (15) applies where r_i now specifies the radius of curvature of a circle into which line segments (defined by cables of length l_i passing from cable guide to cable guide) can be inscribed as illustrated in Figure 10. Likewise, r gives the radius of a circle into which a hypothetical cable of length l_c, which passes through the

center of each segment, can be inscribed.

As shown in Figure 10, a unit of radius $r = \kappa^{-1}$ which bends through θ/n radians (where $\theta = \kappa s$) produces a cable length

$$l_c = 2nr \sin(\theta/2n). \tag{23}$$

Again referring to the figure, the same principle also applies to the per-cable lengths and radii, so that $l_i = 2nr_i \sin(\theta/2n)$. Multiplying (15) by $2n \sin(\theta/2n)$, substituting, and solving gives

$$l_c = l_i + d2n \sin(\theta/2n) \cos\phi_i. \tag{24}$$

In the same manner as the continuously bending actuator case in (17), combining (24) over all three actuators produces

$$l_c = \frac{l_1 + l_2 + l_3}{3}. \tag{25}$$

By the same reasoning, one can apply (24) to two cables and equate the results to yield $d2n \sin(\theta/2n) = (l_2 - l_1)/(\cos\phi_1 - \cos\phi_2)$. The same procedure can then be applied to the second and third cables. Equating and solving gives (18).

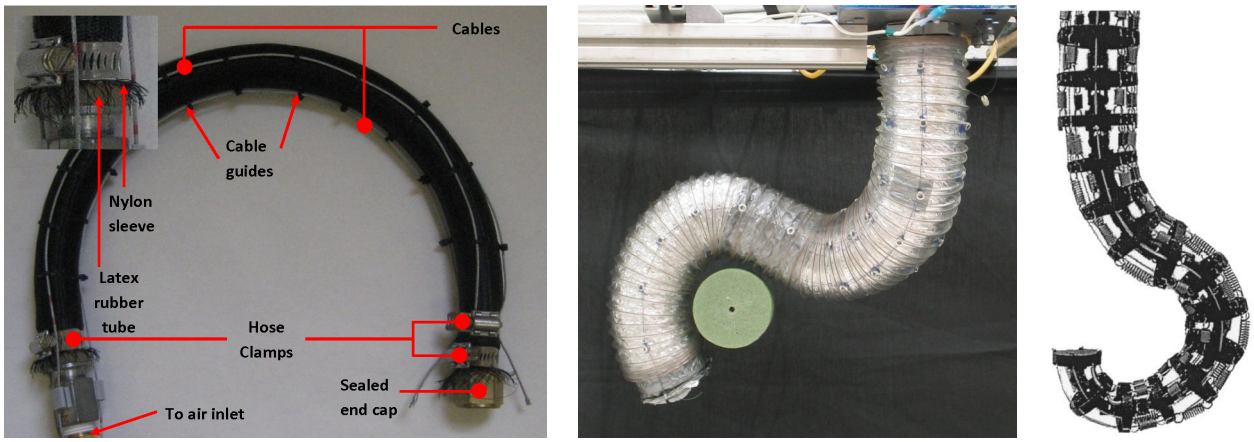

Figure 9: Three examples of cable-driven robots. (Left) A latex rubber tube with three cables at 120° intervals creates an extensible wire-actuated continuum robot [66] (image © [2007] IEEE). (Center) Similarly the Air-OCTOR multisection continuum robot consists of a pressurized hose around which cables are spaced at 120° intervals [49] (image © [2006] IEEE). (Right) The Clemson Elephant Trunk hyperredundant robot [35] consists of a series of U-joints with springs between jointed sections, producing an inextensible robot with approximately constant curvature within each section. Photo courtesy of Ian Walker (image © [1999] IEEE).

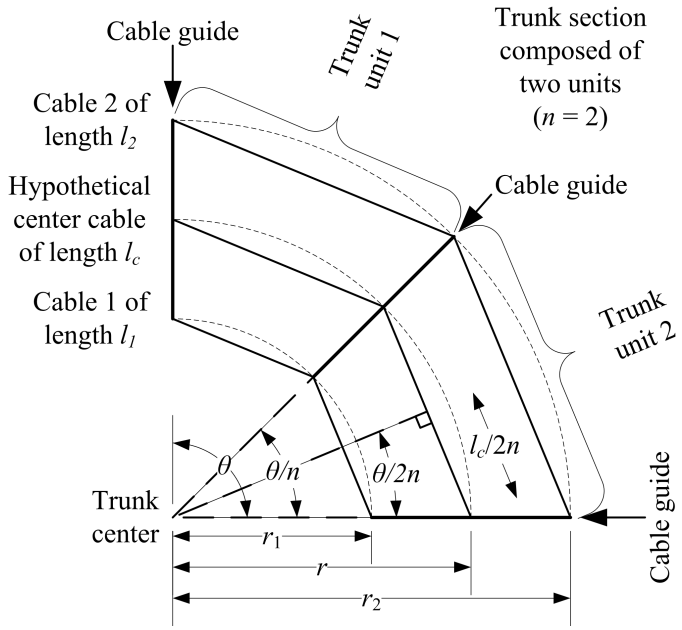

Figure 10: Schematic of a single circular section of a cable-driven continuum robot. This section includes one cable guide (often there are several guides per section) that subdivides it into two units ($n = 2$). This two-dimensional, in-plane view omits one wire for simplicity and shows the special case where the bending plane happens to make the wires equidistant from the central backbone; however, results derived here also apply to general bending planes. The geometry presented shows that $\sin(\theta/2n) = (l_c/2n)/r$, producing (23).

The derivation for $\kappa(\boldsymbol{q})$ is also similar to the procedure described for continuously bending actuation, and yields the same result. This can be derived from (23) and following, which yield $\sin(\theta/2n) = l_c/2nr = l_i/2nr_i$, implying that $r_i = l_i/\kappa l_c$. Equating this with (15) and solving, we obtain $\kappa = (l_c - l_i)/l_c d\cos(\phi_i)$. Choosing $i = 1$ so that $\phi_i = 90° - \phi$ and substituting (25) yields $\kappa = (l_2 + l_3 - 2l_1)/(l_1 + l_2 + l_3)d\sin\phi$. The remainder of the derivation is then identical to the pneumatic case and yields (19).

The arc length of the robot $\ell(\boldsymbol{q})$ can be determined from (23), which yields $\ell = (2n/\kappa)\sin^{-1}(l_c\kappa/2n)$. Applying (19) and (25) yields

$$\ell(\boldsymbol{q}) = \frac{nd(l_1 + l_2 + l_3)}{2\sqrt{l_1^2 + l_2^2 + l_3^2 - l_1l_2 - l_1l_3 - l_2l_3}} \sin^{-1}\left(\frac{\sqrt{l_1^2 + l_2^2 + l_3^2 - l_1l_2 - l_1l_3 - l_2l_3}}{3nd}\right). \quad (26)$$

In summary, the expressions for $\kappa(\boldsymbol{q})$ in (19) and $\phi(\boldsymbol{q})$ in (18) for tendon driven con-

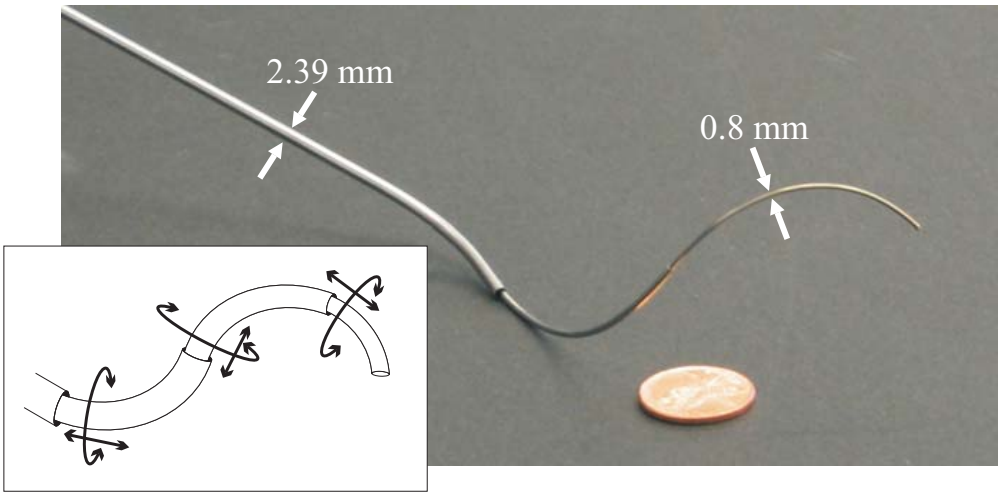

Figure 11: A three-tube active cannula with inset line drawing showing degrees of freedom [106] (image © [2009] IEEE).

tinuum robots are identical to those for the robots with continuously bending actuation described in the previous section. Therefore, (18), (19), and (26) define $\boldsymbol{f}_{specific}$ for these robots. The only difference between the two types, arising from the fact that wires go straight between support discs rather than through curved paths, is in the arc length parameter $\ell(\boldsymbol{q})$ in (26). The four-actuator case follows similarly. Imitating the procedure above but using actuators 1, 3 and 2, 4 as in the continuously bending actuation case yields $\phi(\boldsymbol{q})$ in (21) and $\kappa(\boldsymbol{q})$ in (22). Applying (26) with these updated formulas for ϕ and κ then produces $\ell(\boldsymbol{q})$. See [35] for an alternate derivation.

The inextensibility of many cable-driven robots such as [11, 35, 24, 15] leads to an over-actuated system. Similar to the previous section, (25) prescribes one of the cable lengths when the other two are known, assuming the robot retains a constant-curvature shape. However, additional difficulties arise due to cable extension resulting from loading, which requires examination of the statics of the continuum robot and the resulting forces applied to its cables to properly regulate cable tension, avoid cable slack, and address both under- and over-actuation in these systems [15, 13]. Section 4.2 treats these problems in the more challenging context of a multisection robot.

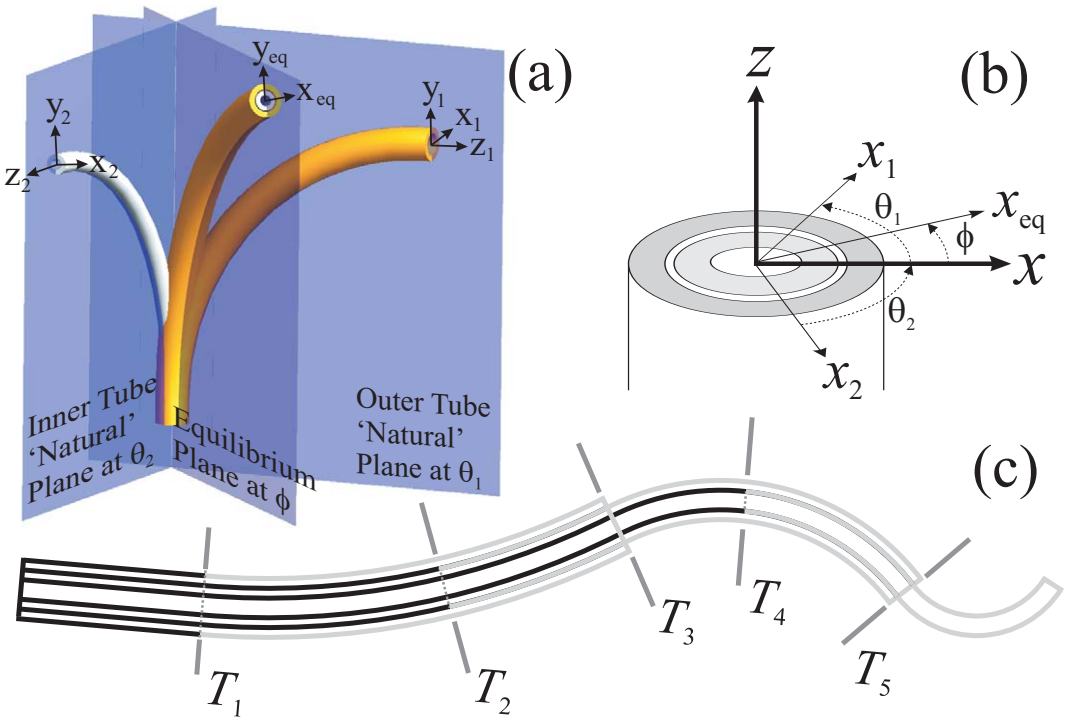

Figure 12: (a) When two circularly precurved tubes are placed concentrically and rotated at their bases, their resultant shape can be approximated by a circular arc lying in a plane between the tubes' individual planes. (b) Cross section showing tube individual frames and equilibrium frame. (c) An active cannula consists of $2n$ such sections for n tubes – black lines denote straight tube segments while gray denote circularly precurved tube segments. Images adapted from [106], original source © [2009] IEEE.

3.2.3 Concentric Tube Continuum Robots

Concentric tube continuum robots, also known as "active cannulas" due to their potential medical applications (Figure 11), are a relatively new type of continuum robot [105, 106, 85, 84, 81, 86, 87, 30]. A distinguishing characteristic of the active cannula design (aside from its small diameter) is that bending actuation is built into the backbone, which is composed of telescoping, precurved elastic tubes. These can be rotated and translated with respect to one another to transmit bending moments.

The joint variables for an active cannula are the translations ($\boldsymbol{\rho}$) and rotations ($\boldsymbol{\theta}$) of component tubes. Thus joint space consists of $\boldsymbol{q} = [\rho_1 \ \theta_1 \ \cdots \ \rho_n \ \theta_n]^{\mathrm{T}}$. Neglecting torsion, actuators at tube bases directly specify tube axial rotation angles at all points along the active cannula.[1] Under this assumption and with circular curvature preformed into each

[1]Note: when torsion is included the shape of an active cannula becomes a general curve, as described in [83, 82, 29, 84, 85, 30], although closed-form solutions are still possible in some cases. This is also true when

component tube, the active cannula consists of piecewise constant curvature links [106, 86] as diagrammed in Figure 12. To determine the arc parameters of a given link, one can apply Bernoulli-Euler beam mechanics. For a collection of tubes with circular precurvatures k_i and a deformed resultant circular curvature common to all tubes κ, moments will be constant along the length of each tube in a given section and can be described by $\kappa - k_i = M/EI$, where M is the bending moment, E is the elastic modulus, and I is the cross sectional inertia of the tube. Writing a moment balance in the equilibrium coordinate frame in component form, one can obtain curvature components of

$$\kappa_x = \frac{\sum_{i=1}^{n} E_i I_i k_i \cos\theta_i}{\sum_{i=1}^{n} E_i I_i} \qquad \kappa_y = \frac{\sum_{i=1}^{n} E_i I_i k_i \sin\theta_i}{\sum_{i=1}^{n} E_i I_i}, \tag{27}$$

where θ_i are the angles input at the base of the link. These can be converted into arc parameters by observing that the equilibrium plane and curvature are

$$\phi(\boldsymbol{q}) = \tan^{-1}\left(\frac{\kappa_y}{\kappa_x}\right) \quad \text{and} \quad \kappa(\boldsymbol{q}) = \sqrt{\kappa_x^2 + \kappa_y^2}, \tag{28}$$

which defines $\boldsymbol{f}_{specific}$ for this type of continuum robot.

Tube transition points (points where tubes either end or transition from straight to curved) bound each link in an active cannula, and together with actuator displacements directly define link lengths through straightforward linear algebraic relationships. The exact functions depend on the order of transition points, and examples and methods for calculation of link lengths are given in [106, 86].

3.2.4 The Steerable Needle

Needles can be "steered" (guided through curved trajectories) inside soft tissue in a variety of ways (for an overview, see [102]). One means of steering needles is to make the needle shaft flexible (e.g., use a material such as Nitinol) and harness the asymmetric forces of a beveled tip. Work in [103] shows that the trajectory of such a bevel-steered needle can be modeled as having piecewise constant curvature. Curves begin and end when the needle is rotated axially, redirecting the bevel and thus the direction of forward progression. A

external forces and moments are applied [81].

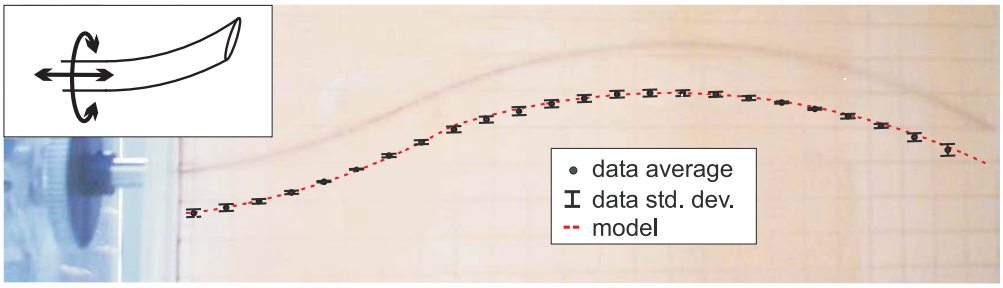

Figure 13: Photo of a steerable needle inserted into simulated muscle, with model prediction superimposed and offset below the needle, so that the needle can be seen.

distinguishing feature of bevel steering is that the backbone (needle shaft) can have as many arcs as desired (a new one begins with each bevel re-orientation), and with constant axial rotation during insertion steerable needles can also achieve helical trajectories. However, in contrast to other continuum robots, only arcs forward of the current tip position can be affected by the actuators. Arcs embedded in tissue will stay in place with constant arc parameters, regardless of actuator motion, because they are held by the tissue [104]. When retracted, the needle will return along the path through which it entered the tissue.

Steerable needle kinematics can be described by considering body velocity. The body frame twist coordinates corresponding to insertion and rotation of the needle are the same as those given in (10)-(11), namely,[2]

$$\boldsymbol{\xi}_{\text{rotation}} = \begin{bmatrix} 0 & 0 & 0 & 0 & 0 & 1 \end{bmatrix}^{\mathrm{T}} \text{ and}$$
$$\boldsymbol{\xi}_{\text{insertion}} = \begin{bmatrix} 0 & 0 & 1 & 0 & \kappa & 0 \end{bmatrix}^{\mathrm{T}}.$$

Converting these to twists, we have

$$\widehat{\boldsymbol{\xi}}_{\text{insertion}} = \begin{bmatrix} \kappa\widehat{\boldsymbol{e}}_2 & \boldsymbol{e}_3 \\ 0 & 0 \end{bmatrix} \qquad \widehat{\boldsymbol{\xi}}_{\text{rotation}} = \begin{bmatrix} \widehat{\boldsymbol{e}}_3 & 0 \\ 0 & 0 \end{bmatrix}, \tag{29}$$

where $\boldsymbol{e}_i$ are standard basis vectors and the $\widehat{\ }$ notation is used as in (12).

[2]Note that the insertion twist given here is slightly different than the $\xi_{\text{insertion}} = \begin{bmatrix} 0 & 0 & 1 & \kappa & 0 & 0 \end{bmatrix}^{\mathrm{T}}$ given in [103] to be consistent with the frame convention used throughout this paper.

If the sequence (and distances) of insertion and rotation motions for a complete needle trajectory are known *a priori*, the product of exponentials formula can be applied directly in a similar manner to (13), as $\mathrm{T} = e^{(\widehat{\boldsymbol{\xi}}_{\text{insertion}}\ell_1)}e^{(\widehat{\boldsymbol{\xi}}_{\text{rotation}}\phi_1)}\dots e^{(\widehat{\boldsymbol{\xi}}_{\text{insertion}}\ell_n)}e^{(\widehat{\boldsymbol{\xi}}_{\text{rotation}}\phi_n)}$.[3] However, normally the input degrees of freedom will be dynamically manipulated by a control system, in which case the forward translation of the needle will be given by

$$\dot{\mathrm{T}}(t) = \mathrm{T}(t)\left(u_1\widehat{\boldsymbol{\xi}}_{\text{insertion}} + u_2\widehat{\boldsymbol{\xi}}_{\text{rotation}}\right), \tag{30}$$

where u_1 and u_2 are the insertion and rotation velocity inputs, respectively, applied at the needle base. When the needle is used under closed loop control with feedback from a medical imaging system, a needle controller (e.g. [52]) determines u_1 and u_2 in real-time and applies them using motors connected to the needle base (see [104, 76]). To determine needle pose, (30) can be integrated (see [103] for details and [73] for an in-depth discussion on several numerical integration techniques) to determine needle pose.

4 Multisection Forward and Inverse Kinematics

4.1 Forward Kinematics

Many continuum robot applications require multi-section robots, in order to provide a sufficient number of degrees of freedom for task requirements. Since a single section generally provides two or three degrees of freedom, positioning the robot's tip with 6 DOF requires a minimum of two to three sections, and more are desirable to increase workspace size and provide redundant solutions. Actuator length limits can also constrain single-section robot motion to a subspace of the theoretical workspace, producing a relatively small workspace for many single-section manipulators (see [50] for one example). Furthermore, whole-arm grasping and the ability to work in cluttered environments often require one or more sections dedicated to the task, while other sections toward the robot's base support and position dis-

[3] The order of exponentials within each pair describing a section is reversed here, with respect to (13), because the axial rotation at the end of the i$^{\text{th}}$ link affects the plane of link $i+1$.

tal sections. All of these factors provide ample motivation for multi-section robots; indeed, many of the existing designs listed on Table 1 are equipped with multiple sections.

However, multi-section continuum robots can introduce additional complexity in the mappings illustrated in Figure 2. In general, the robot-independent forward kinematic results are straightforward to generalize to the multi-section case. One simple way to see this is to consider each section as having its own transformation (equations (1) or (2) when expressed using the homogeneous matrix representation), then simply multiplying these transformations as one would for traditional serial robot link transformations. However, the robot-specific mapping cannot always be so cleanly decoupled, and doing so sometimes requires consideration of the whole robot and simultaneous solution of all sections.

In terms of the example designs given in Section 3.2, the cables and push-rods that actuate distal sections of the robot (those toward the robot's tip) pass through and therefore affect the shape of proximal sections, requiring a whole-robot solution. In contrast, the latex rubber tubes in pneumatically-actuated robots terminate at each section boundary, producing a mechanically decoupled design solvable on a per-section basis. While distal sections in concentric-tube continuum robots also pass through proximal sections and affect their shape, this coupling is directly built into the model as expressed in Section 3.2.3. For the steerable needle, there is no coupling, and each section in an *a priori* determined actuator trajectory does not affect other sections.

Thus, the designs where extension to multiple sections requires additional analysis are those involving push rods and cables. Referring to Figure 14, co-located actuators provide a straightforward method to determine distal actuator length as the sum of all co-located proximal actuators. For example, the robot in [112] features hollow push rods, in which distal rods lie inside proximal rods. In the more common case of distributed actuation, the length of a distal actuator must be computed by referring to the arc parameters for proximal sections then using a single-section mapping to compute these lengths as they pass through each proximal section, a process termed "tangle/untangle" in [50]. If actuator forces cause compression of the robot and extension of the actuating cables, a consideration of statics

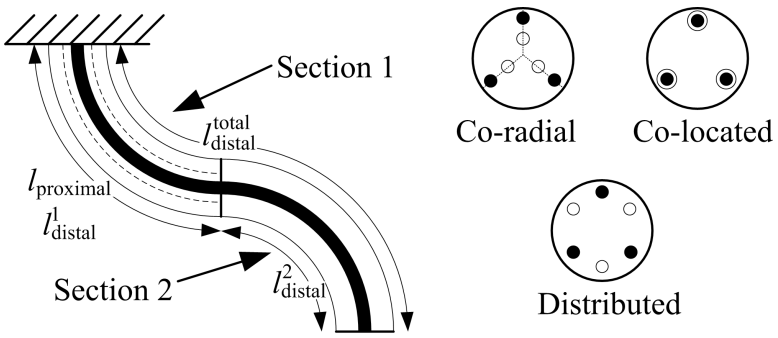

Figure 14: A two-section robot illustrates the "tangle/untangle" process. Co-located concentric proximal and distal actuators (as is the case with the flexible push-rod design – the sketch above indicates actuators that pass directly through one another) simplify the process because the section lengths of all rods – both those that actuate the base and tip section – passing through the base section are identical. When cables for multiple sections lie at equal angles about the central axis of the device (termed "co-radial" above), a slightly more complex process of mapping outer actuator lengths to shape, and then back to inner actuator lengths, decouples the actuator lengths. In the most complex case for multi-section cable-driven designs, where the cables for proximal and distal sections cannot be coaxial (and are therefore distributed around the edge of each disc), an iterative procedure known as tangle/untangle [50] or a statics model with optimization [13] can be used to determine multi-section cable lengths.

can enable calculation of cable lengths [13].

4.2 Inverse Kinematics

As with all serial robots, and particularly in the case of redundant robots, inverse kinematics is challenging. For a constant curvature continuum robot, one usually begins by computing the inverse mapping between task space and configuration space (the robot-independent inverse mapping). This produces the arc parameters of all sections of the robot, which correspond to the desired tip pose. Computing all possible solutions to this problem for a continuum robot with a large number of sections is clearly not trivial, but several approaches for inverse kinematics do exist. A closed-form geometric approach is given for single and multiple sections in [65], based on modeling each section using a spherical joint and a straight rigid link, then applying an analytical process to solve inverse kinematics for this model before converting back to arc parameters. This approach provides simple access to the entire solution space of the rigid-link robot and can easily be applied to an n-link robot. However, this formulation does not yet account for physical actuation limits, such as limited

actuator lengths, forces, or locations.

The Jacobian (see Section 5.1) provides another approach to robot-independent inverse kinematics. It finds a single solution to the problem by servoing a virtual copy of the robot from any initial guess (including the robot's current configuration) to the desired configuration (see e.g. [87, 107] for active cannula results). In this Jacobian-based inverse kinematics strategy, it is possible to build actuator limits into the control law so that the robot's trajectory is always physically realizable.

The inverse mapping from arc parameters to actuator parameters differs for each kind of continuum robot, similar to the forward mapping. Bevel-steered needle inverse kinematics are the most straightforward, since the desired ϕ for each section directly defines the amount of axial rotation necessary after each forward translation along the previous section. Inverse kinematics of concentric-tube continuum robots are only slightly more complex, given a set of arc parameters in their workspace. For these robots, one can work backward from the distal section (see Figure 12), where ϕ_n is equivalent to the axial angle of the single tube it contains. The second-to-last section contains two tubes, so given its arc parameters and the fact that we have already determined the axial angle of one of the two tubes it contains, (27) and (28) have only one unknown, and can be solved in closed form for a second axial tube angle. Repeating this procedure for each subsequent section as one moves toward the robot's base, one tube angle is completely defined by each section.

Additional single-section inverse mappings from arc parameters to actuator parameters include derivations for push rod-actuated robots [112] and for single-section cable and pneumatically-actuated robots [49]. Using these mappings, [50] produces an analytical derivation of the workspace of these robots under actuator length limit constraints and describes a "tangle/untangle" algorithm for multi-section cable-actuated robots with actuators equally spaced about the base of the trunk.

The above algorithms restrict their attention to constant-curvature kinematics, and thus do not include real-world effects that can be important in some continuum robot designs such as gravitational loading or friction. For example, friction can cause non-circular

deformation in the flexible push-rod design. Fortunately, this can be overcome by compensation that makes use of redundant actuation in the single [111] and multi-section cases [90]. Likewise, some continuum robot designs undergo appreciable axial compression due to actuator forces, necessitating a static analysis of the system to compute cable lengths which correspond to desired arc parameters [13].

5 Differential Kinematics

One approach to derive the Jacobian matrix for a continuum robot is to compute the full kinematics as described in Section 3 using both the system specific and system independent mappings, then to directly differentiate the components of the resulting homogeneous transformation (see e.g. [49, 35]). While this is conceptually straightforward, in practice it can become computationally cumbersome. A multi-section robot would require multiplication of several copies of (2) or (3) and substitution of potentially lengthy robot-specific definitions of arc parameters, such as those derived in Section 3.2.

However, a robot-specific/robot-independent approach similar to that taken with forward kinematics earlier in this paper can also be applied to differential kinematics [107]. To accomplish this, first observe that forward kinematics is a composition of maps, namely $\mathrm{T} = \mathrm{T}(\boldsymbol{\kappa}(\boldsymbol{q}), \boldsymbol{\phi}(\boldsymbol{q}), \boldsymbol{\ell}(\boldsymbol{q}))$. This implies that we can use the chain rule to compute differential kinematics.

5.1 Robot-Independent Jacobian

At first glance, applying the chain rule to (13) is not straightforward, because both $\kappa(\boldsymbol{q})$ and $\ell(\boldsymbol{q})$ appear in the second exponential. However, following [107], we begin by computing spatial velocity for one section (the j^{th} section) of a continuum robot as

$$\widehat{V}_j^s = \dot{T}_j T_j^{-1} = \widehat{\boldsymbol{e}}_6 \Delta\dot{\phi}_j + e^{\widehat{\boldsymbol{e}}_6 \Delta\phi_j} \left(\frac{d}{dt} e^{(\widehat{\boldsymbol{e}}_3 + \widehat{\boldsymbol{e}}_4 \kappa_j)\ell_j} \right) T_j^{-1}, \tag{31}$$

where T_j is given in (13) but with ϕ_j replaced with $\Delta\phi_j = \phi_j - \phi_{j-1}$ to enable the result to be used with a multi-section robot. Using trigonometric series it can be shown that the final term of (31) reduces to $e^{\widehat{\boldsymbol{e}}_6\Delta\phi_j}\widehat{A}_j e^{-\widehat{\boldsymbol{e}}_6\Delta\phi_j}$, where

$$\widehat{A}_j = \begin{bmatrix} \widehat{\boldsymbol{e}}_2\dot{\kappa}_j\ell_j & \left(\dot{\ell}_j + \frac{\dot{\kappa}_j(\kappa_j\ell_j - \sin(\kappa_j\ell_j))}{\kappa_j^2}\right)\boldsymbol{e}_3 + \frac{\dot{\kappa}_j(\cos(\kappa_j\ell_j)-1)}{\kappa_j^2}\boldsymbol{e}_1 \\ 0 & 0 \end{bmatrix}.$$

Converting (31) from $\mathfrak{se}(3)$ to $\mathbb{R}^6$ yields $V_j^s = \boldsymbol{e}_6\Delta\dot{\phi}_j + \mathrm{Ad}_{e^{\widehat{\boldsymbol{e}}_6\Delta\phi_j}}A_j$, which reduces to

$$V_j^s = \underbrace{\begin{bmatrix} \cos\Delta\phi_j(\cos(\kappa_j\ell_j)-1)/\kappa_j^2 & 0 & 0 \\ \sin\Delta\phi_j(\cos(\kappa_j\ell_j)-1)/\kappa_j^2 & 0 & 0 \\ -(\sin(\kappa_j\ell_j)-\kappa_j\ell_j)/\kappa_j^2 & 0 & 1 \\ -\ell_j\sin\Delta\phi_j & 0 & -\kappa_j\sin\Delta\phi_j \\ \ell_j\cos\Delta\phi_j & 0 & \kappa_j\cos\Delta\phi_j \\ 0 & 1 & 0 \end{bmatrix}}_{J_j^s} \begin{bmatrix} \dot{\kappa}_j \\ \Delta\dot{\phi}_j \\ \dot{\ell}_j \end{bmatrix}. \tag{32}$$

Note that J_j^s is well defined for all $(\kappa_j, \Delta\phi_j, \ell_j)$, even in the the limit as κ_j approaches 0.

Given this single-section Jacobian, one can generalize to multiple sections by expressing individual section Jacobians in the spatial frame. Applying the relevant adjoint transformations,

$$J_{robot}^s = \begin{bmatrix} J_0 & \mathrm{Ad}_{\mathrm{T}_0}J_1 & \mathrm{Ad}_{\mathrm{T}_{01}}J_2 & \cdots & \mathrm{Ad}_{\mathrm{T}_{0(m-1)}}J_m \end{bmatrix} \tag{33}$$

where J_j is the j^{th} section Jacobian (32), and $\mathrm{T}_{0j} = \mathrm{T}_0\mathrm{T}_1\cdots\mathrm{T}_j$. This result can then be used to determine the spatial velocity (see [63] for an in-depth discussion of the proper interpretation of spatial and body velocities) of the tool frame by multiplying it on its right by a vector consisting of a stack of all m triplets of arc parameter velocities.

5.2 Robot-Specific Derivatives

Some continuum robots permit direct control of arc parameters. With such robots, the robot-independent result above can be directly applied. In others, including some of our examples in Section 3.2, the mapping between joint variables and arc parameters may be written in closed form (see e.g. [7, 49, 87]). When this is possible, one can directly differentiate the expressions for the arc parameters. In still other cases, including active cannulas when they are approximated as piecewise constant curvature as in [106], obtaining arc parameters requires numerical energy minimization. Even this does not necessarily preclude a closed-form Jacobian. It has been shown in [107] that by applying a local version of the implicit function theorem, one can arrive at a closed-form Jacobian for an active cannula. Efficient methods for obtaining the Jacobian for non-circular continuum robots, including piecewise constant curvature robots of all designs under significant external loading (as well as active cannulas with variable precurvature and/or under external loading [81]) is an open research question that is discussed below in terms of future challenges in the field of continuum robots.

6 Opportunities For Future Research

The efforts of many researchers have led to significant advancements in the design, application, and theoretical foundation for continuum robotics, as has been reviewed in previous sections of this paper. However, before continuum robots become as pervasive as their rigid-link counterparts, a number of ongoing research challenges must be addressed. Here, we discuss several of the many themes that will be important in the future of continuum robotics research.

6.1 Design

The diversity of applications and sizes of continuum robots provide fertile ground for design innovation, as can be clearly seen from the examples in Section 2. The coupling of actuation and elastic support structure is an active area of research, as are the tradeoffs between distributed, discrete, and remote (e.g. cable) actuation, and the best combinations of these strategies. Related to this are the challenges of concatenating multiple sections (the actuators for distal sections can often influence the shape of proximal ones as described in Section 4.2), appropriately tuning or controlling overall robot stiffness to match application objectives, and identifying and using robust materials with long functional lifetimes. Similarly, it is not always clear how to incorporate actuator or structural limits (see e.g. [48]) into models to prevent robot self-damage or damage under load. Furthermore, many of the continuum robots developed to date have not yet been fitted with end effectors. Depending on design, weight, and actuation, these end effectors may require mechanical or algorithmic compensation for their effect on robot shape. Each of the above factors provide researchers with many opportunities for innovation in continuum robot design when approaching each new application.

6.2 Static Modeling

As we have described in this paper, the piecewise constant curvature approximation is often useful and has been widely applied. However, general methods to characterize the error induced by this assumption do not currently exist. The common approach to justify the assumption is to (1) photograph the robot and observe that a circle fits the actual backbone shape "rather well," (2) proceed with the subject matter of the paper (design, kinematics, application requirements, etc.), (3) experimentally assess overall performance of the entire robot system, and (4) conclude that if the experiments were successful then the piecewise constant curvature approximation was sufficiently accurate. This process does not provide an early means of testing a single section of the robot to extrapolate whether a multisection robot will be likely to meet design requirements. Thus, general results on error propagation based

on metrics for the circularity (or lack thereof) of the physical robot shape would be valuable. Furthermore, in cases where piecewise constant curvature is not sufficient, advancements will be needed in working with more complex variable curvature models. There is a great deal of current interest in obtaining deeper understanding of the fundamental mechanics of continuum robots in terms of general theories of elasticity, and both energy minimization (see e.g. [85], among others) and Cosserat rod theory (see e.g. [98, 30, 81], among others) have yielded useful recent results. The ability to include the effects of gravity, torsion, and external loading in such models is particularly useful. Based on the current trajectory of this area of research, it appears likely that advancements will first come in the form of general models that account for these effects, and researchers will then seek parsimonious simplifications that capture salient features and are sufficiently accurate and efficient for use in real-time control.

6.3 Dynamic Modeling

In this paper we have reviewed static modeling results for constant curvature robots. A particularly challenging emerging area of research involves deriving and practically applying dynamic models of continuum robots in a numerically stable form amenable to real-time implementation. The dynamic equations of continuum robots under various assumptions have been derived in the planar case [33, 95] and derivations based on an energy-work relationship [45], conservation laws [19], and a Newtonian formulation of Cosserat rods [98] exist. We note that some of the earliest, yet most advanced work in terms of practical implementation is that of is the work of Chrikjian [19] where a variable geometry truss provided a means of computing planar continuum robot dynamics rapidly. We note also that several non-robotic applications of Cosserat rod dynamics address these issues [91, 56] and show promise for future application in continuum robotics. In summary, efficient implementation of dynamic models for various kinds of continuum robots is an open and active area of research. It is likely that over the next few years dynamic models will become increasingly more general (many existing formulations are done in 2D and/or assume constant curvature), and that

increasingly efficient and stable numerical techniques for real-time implementation will be developed, both of which facilitate the practical application of continuum robots in dynamic environments that require rapid motion.

6.4 Sensing, Control, and Calibration

Traditional encoders are not generally sufficient for determining continuum robot shape, since continuum robots have an infinite number of degrees of freedom (they bend continuously). However, feedback on robot shape is necessary to enable closed-loop control. This has lead several researchers to explore computer vision for shape sensing (see e.g. [22, 14, 25]) and visual servo control. Developing imaging methods that are both accurate and efficient will be a key to real-time control. Control advancements may include methods of servoing the entire shape of the robot curve to a desired curve. Promising sensing possibilities other than computer vision include embedded strain gages or fiber optic techniques such as ShapeTape [60], while medical systems will likely employ intraoperative medical imaging. Such medical imaging may be similar to optical cameras (e.g. biplane fluoroscopy), or provide direct 3D information (e.g. 3D ultrasound [12]). We note also that in addition to control, sensors can be used for robot calibration, enabling fitting of imprecisely known robot parameters (e.g. stiffnesses, lengths, etc.) to experimental data. This can be done in a variety of ways with many different sensors and continuum robot types, and [106] and [112] provide two specific examples this technique.

6.5 Complete systems

Complete integrated systems are likely to include user interfaces and must address efficiency in order to implement the computations relating to robot motion in real time (see e.g. [50]). It is not yet clear what the optimal kinematic mappings between human user input and the curve of a continuum robot will be, although some promising initial studies have been done (see e.g. [26, 42]). With regard to efficiency, deriving closed-form inverse kinematics (e.g.

[65, 80, 87]) may provide an alternative to Jacobian-based techniques, and one must also address limiting cases in a computationally robust way [51]. Furthermore, advancements are needed in motion planning and obstacle avoidance for continuum robots (see [59] for one approach). We also note that these topics have been addressed for hyperredundant robots (see e.g. [35] and [23]). Continuum robots also offer the possibility to manipulate objects with the whole arm [10, 61], which can help the robot to securely grasp objects whose geometry or position is imprecisely known. In medical applications complete systems will include use of preoperative and intraoperative image data, statistical information about anatomical geometry, appropriate and interchangeable end effectors, human interfaces, and assistance that can be provided to the doctor in the form of virtual fixtures [53].

7 Conclusion

Continuum robots have been adopted in a wide variety of applications, as discussed in Section 2, and are becoming increasingly valuable tools for the robotics community. Precisely because their most useful characteristics (dexterity in cluttered and unstructured environments, gentle and compliant interaction with objects, etc.) differ from those of traditional robots (rigidity, precision, suitability for highly structured environments), they require corresponding advancements in robotics theory. As reviewed in this paper, the most general models describing continuum robot shape (forward kinematics) involve numerical integration. Thus, in order to achieve closed-form results and thus facilitate real-time control, differential kinematics, inverse kinematics, etc., many researchers have applied the closed-form piecewise constant curvature approximation and found it to be sufficiently accurate for their objectives.

Herein, we have reviewed the many mechanical continuum robot architectures for which the piecewise constant curvature approximation has been found applicable. Further, we described important results in piecewise constant curvature kinematics, setting them in a single coordinate frame and notational convention and indicating which results are robot-specific

and which are robot-independent. The latter may be applied directly to each new (approximately) piecewise constant curvature continuum robot design developed in the future.

In summary, continuum robots offer the potential to extend the benefits of robotics to applications that have not previously been approachable with robots. These include working in unstructured or constrained environments and manipulating delicate objects or those with imprecisely known shapes or locations. The study of continuum robotics is entering an exciting era. While useful general results such as those reviewed in this paper have been developed, there remain many avenues for future research and many promising new applications that have not yet been explored. Given the accelerating pace of fundamental progress in design, modeling, and practical implementation, continuum robots appear poised to become increasingly useful tools that will play key roles in the future of robotics.

Acknowledgement

This work was funded in part by the National Science Foundation under grant # 0651803 and by Vanderbilt and Mississippi State Universities.

References

[1] V. Anderson and R. Horn. Tensor arm manipulator design. *ASME Transactions*, 67-DE-57(2):1–12, 1967. (paper)

[2] V. Anderson and R. Horn. Tensor arm manipulator, Feb. 1970. U.S. Patent 3,497,083. (paper)

[3] S. B. Andersson. Discretization of a continuous curve. *IEEE Transactions on Robotics*, 24(2):456 – 461, 2008. doi:10.1109/TRO.2008.917000. (paper)

[4] S. S. Antman. *Nonlinear Problems of Elasticity*, volume 107 of *Applied Mathematical Sciences*. Springer, New York, NY, 2nd edition, 2005.

[5] T. Aoki, A. Ochiai, and S. Hirose. Study on slime robot: development of the mobile robot prototype model using bridle bellows. In *IEEE International Conference on Robotics and Automation*, volume 3, pages 2808–2813, April 2004. doi:10.1109/ROBOT.2004.1307486. (paper)

[6] T. Aoki, H. Ohno, and S. Hirose. Design of slim slime robot II (SSR-II) with bridle bellows. In *IEEE/RSJ International Conference on Intelligent Robots and System*, volume 1, pages 835–840, October 2002. doi:10.1109/IRDS.2002.1041494. (paper)

[7] Y. Bailly and Y. Amirat. Modeling and control of a hybrid continuum active catheter for aortic aneurysm treatment. In *IEEE International Conference on Robotics and Automation*, pages 936–941, April 2005. (paper)

[8] R. L. Bishop. There is more than one way to frame a curve. *The American Mathematical Monthly*, 82:246–251, 1975. (paper)

[9] R. V. Bostelman, J. S. Albus, and R. E. Graham. Robocrane and EMMA applied to waste storage tank remediation. In *American Nucelar Society Seventh Topical Meeting on Robotics and Remote Systems*, volume 2, pages 708–713, 1997. (paper)

[10] D. Braganza, M.L. McIntyre, D.M. Dawson, and I.D. Walker. Whole arm grasping control for redundant robot manipulators. In *American Control Conference*, pages 3194–3199, June 2006. doi:10.1109/ACC.2006.1657209. (paper)

[11] R. Buckingham. Snake arm robots. *Industrial Robot: An International Journal*, 29(3):242–245, 2002. doi:10.1108/01439910210425531. (paper)

[12] E. C. Burdette, D. C. Rucker, P. Prakash, C. J. Diederich, J. M. Croom, C. Clarke, P. Stolka, T. Juang, E. M. Boctor, and R. J. Webster III. The ACUSITT ultrasonic ablator: The first steerable needle with an integrated interventional tool. *Proceedings of SPIE Medical Imaging*, 2010. (In Press).

[13] D. B. Camarillo, C. R. Carlson, and J. K. Salisbury. Configuration tracking for continuum manipulators with coupled tendon drive. *IEEE Transactions on Robotics*, 25(4):798–808, 2009. doi:10.1109/TRO.2009.2022426. (paper)

[14] D. B. Camarillo, C. R. Carlson, and J. K. Salisbury. Task-space control of continuum manipulators with coupled tendon drive. *11th International Symposium on Experimental Robotics 2008, Springer Tracts in Advanced Robotics*, 54:271–280, 2009. doi:10.1007/978-3-642-00196-3_32. (paper)

[15] D. B. Camarillo, C. F. Milne, C. R. Carlson, M. R. Zinn, and J. K. Salisbury. Mechanics modeling of tendon-driven continuum manipulators. *IEEE Transactions on Robotics*, 24(6):1262 – 1273, 2008. doi:10.1109/TRO.2008.2002311. (paper)

[16] G. Chen, M. T. Pham, T. R. Herve, and C. Prelle. Design and modeling of a micro-robotic manipulator for colonoscopy. In *5th Intl. Workshop on Research and Education in Mechatronics*, pages 109–114, Annecy, France, 2005. (paper)

[17] G. Chen, M. T. Pham, and T. Redarce. Development and kinematic analysis of a silicone-rubber bending tip for colonoscopy. In *IEEE/RSJ International Conference on Intelligent Robots and Systems*, pages 168–173, Oct. 2006. doi:10.1109/IROS.2006.282129. (paper)

[18] G. Chen, G. Thomann, M.T. Pham, M. Betemps, and T. Redarce. Modeling and control of a colonoscopic tip under disturbance of the insertion of colonoscope. In *IEEE/RSJ International Conference on Intelligent Robots and Systems*, volume 4, pages 3315–3320, Sept. 2004. doi:10.1109/IROS.2004.1389928. (paper)

[19] G. S. Chirikjian. Hyper-redundant manipulator dynamics: A continuum approximation. *Advanced Robotics*, 9(3):217–243, 1995. (paper)

[20] G. S. Chirikjian and J. W. Burdick. A modal approach to hyper-redundant manipulator kinematics. *IEEE Transactions on Robotics and Automation*, 10(3):343–353, June 1994. doi:10.1109/70.294209. (paper)

[21] G.S. Chirikjian and J.W. Burdick. Kinematically optimal hyper-redundant manipulator configurations. *IEEE Transactions on Robotics and Automation*, 11(6):794–806, Dec 1995. doi:10.1109/70.478427. (paper)

[22] V. K. Chitrakaran, A. Behal, D. M. Dawson, and I. D. Walker. Setpoint regulation of continuum robots using a fixed camera. *Robotica*, 25(5):581–586, 2007. doi:10.1017/S0263574707003475. (paper)

[23] H. Choset and W. Henning. A follow-the-leader approach to serpentine robot motion planning. *ASCE Journal of Aerospace Engineering*, 12(2):65–73, April 1999. doi:10.1061/(ASCE)0893-1321(1999)12:2(65). (paper)

[24] R. Cieślak and A. Morecki. Elephant trunk type elastic manipulator - a tool for bulk and liquid materials transportation. *Robotica*, 17(01):11–16, 1999. doi:10.1017/S0263574799001009. (paper)

[25] J. M. Croom, D. C. Rucker, J. M. Romano, and R. J. Webster III. Visual sensing of continuum robot shape using self-organizing maps. *IEEE International Conference on Robotics and Automation*. (In Press).

[26] M. Csencsits, B. A. Jones, W. McMahan, V. Iyengar, and I. D. Walker. User interfaces for continuum robot arms. *IEEE/RSJ International Conference on Intelligent Robots and Systems*, pages 3123– 3130, 2005. doi:10.1109/IROS.2005.1545434. (paper)

[27] P. Dario, M. C. Carrozza, M. Marcacci, S. D'Attanasio, B. Magnami, O. Tonet, and G. Megali. A novel mechatronic tool for computer-assisted arthroscopy. *IEEE Transactions on Information Technology in Biomedicine*, 4(1):15–29, 2000. doi:10.1109/4233.826855. (paper)

[28] A. Degani, H. Choset, A. Wolf, T. Ota, and M. A. Zenati. Percutaneous intrapericardial interventions using a highly articulated robotic probe. In *IEEE / RAS-EMBS International Conference on Biomedical Robotics and Biomechatronics*, pages 7 – 12, February 2006. doi:10.1109/BIOROB.2006.1639051. (paper)

[29] P. E. Dupont, J. Lock, and E. Butler. Torsional kinematic model for concentric tube robots. In *IEEE International Conference on Robotics and Automation*, pages 3851 – 3858, Kobe, Japan, May 2009. (paper)

[30] P. E. Dupont, J. Lock, B. Itkowitz, and E. Butler. Design and control of concentric tube robots. *IEEE Transactions on Robotics*, 2010. (In Press).

[31] I. Ebeert-Uphoff and G. Chirikjian. Inverse kinematics of discretely actuated hyper-redundant manipulators using workspace densities. In *IEEE International Conference on Robotics and Automation*, pages 139–145, April 1996. doi:10.1109/ROBOT.1996.503586. (paper)

[32] I. A. Gravagne. *Design, Analysis and Experimentation: the Fundamentals of Continuum Robotic Manipulators*. PhD thesis, Clemson University, 2002. (paper)

[33] I. A. Gravagne, C.D. Rahn, and I. D. Walker. Large-deflection dynamics and control for planar continuum robots. *IEEE/ASME Transactions on Mechatronics*, 8(2):299–307, June 2003. doi:10.1109/TMECH.2003.812829. (paper)

[34] I. A. Gravagne and I. D. Walker. Manipulability, force, and compliance analysis for planar continuum robots. *IEEE Transactions on Robotics and Automation*, 18(3):263–273, June 2002. doi:10.1109/TRA.2002.1019457. (paper)

[35] M. W. Hannan and I. D. Walker. Kinematics and the implementation of an elephant's trunk manipulator and other continuum style robots. *Journal of Robotic Systems*, 20(2):45–63, 2003. (paper)

[36] K. Harada, Zhang Bo, S. Enosawa, T. Chiba, and M.G. Fujie. Bending laser manipulator for intrauterine surgery and viscoelastic model of fetal rat tissue. In *IEEE International Conference on Robotics and Automation*, pages 611–616, April 2007. doi:10.1109/ROBOT.2007.363054. (paper)

[37] S. Hirose. *Biologically Inspired Robots, Snake-Like Locomotors and Manipulators*. Oxford University Press, 1993.

[38] S. Hirose and S. Ma. Coupled tendon-driven multijoint manipulator. In *IEEE International Conference on Robotics and Automation*, volume 2, pages 1268–1275, April 1991. doi:10.1109/ROBOT.1991.131786. (paper)

[39] S. Hirose and H. Yamada. Snake-like robots. *IEEE Robotics & Automation Magazine*, 16(1):88 – 98, 2009. doi:10.1109/MRA.2009.932130. (paper)

[40] K. Ikuta, M. Tsukamoto, and S. Hirose. Shape memory alloy servo actuator system with electric resistance feedback and application for active endoscope. In *IEEE International Conference on Robotics and Automation*, pages 427–430, April 1988. doi:10.1109/ROBOT.1988.12085. (paper)

[41] G. Immega. Tentacle-like manipulators with adjustable tension lines, June 7 1994. U. S. Patent 5,317,952. (paper)

[42] G. Immega and K. Antonelli. The KSI tentacle manipulator. In *IEEE International Conference on Robotics and Automation*, volume 3, pages 3149–3154, May 1995. doi:10.1109/ROBOT.1995.525733. (paper)

[43] G. Immega, K. Antonelli, and J. Ko. Teleoperation of the KSI tentacle manipulator for hot cell decontamination. In *Proceedings of the IEEE International Conference on Intelligent Systems for the 21st Century*, volume 3, pages 2133–2136, Vancouver, Canada, October 1995. doi:10.1109/ICSMC.1995.538095. (paper)

[44] Temple Allen Industries. http://www.templeallen.com/.

[45] M. Ivanescu, M. C. Florescu, N. Popescu, and D. Popescu. Coil function control problem for a hyperredundant robot. In *IEEE/ASME International Conference on Advanced Intelliget Mechatronics*, pages 1–6, Sept. 2007. doi:10.1109/AIM.2007.4412492. (paper)

[46] M. Ivanescu and V. Stoian. A variable structure controller for a tentacle manipulator. In *Proceedings of the IEEE International Conference on Robotics and Automation*,

volume 3, pages 3155–3160, Nagoya, Japan, 1995. doi:10.1109/ROBOT.1996.509277. (paper)

[47] B. A. Jones, R. Gray, and K. Turlapati. Real-time statics for continuum robots. In *IEEE/RSJ International Conference on Intelligent Robots and Systems*, pages 2659 – 2664, St. Louis, MO, USA, October 2009. (paper)

[48] B. A. Jones, W. McMahan, and I. D. Walker. Practical kinematics for real-time implimentation of continuum robots. *IEEE International Conference on Robotics and Automation*, pages 1840–1847, May 2006. (paper)

[49] B. A. Jones and I. D. Walker. Kinematics for multisection continuum robots. *IEEE Transactions on Robotics*, 22(1):43–55, Feb. 2006. (paper)

[50] B. A. Jones and I. D. Walker. Practical kinematics for real-time implementation of continuum robots. *IEEE Transactions on Robotics*, 22(6):1087–1099, Dec. 2006. doi:10.1109/TRO.2006.886268. (paper)

[51] B. A. Jones and I. D. Walker. Limiting-case analysis of continuum trunk kinematics. *IEEE International Conference on Robotics and Automation*, pages 1363 – 1368, 2007. doi:10.1109/ROBOT.2007.363174. (paper)

[52] V. Kallem and N. J. Cowan. Image guidance of flexible tip-steerable needles. *IEEE Transactions on Robotics*, 25:191–196, 2009. doi:10.1109/TRO.2008.2010357. (paper)

[53] A. Kapoor. *Motion Constrained Control of Robots for Dexterous Surgical Tasks*. PhD thesis, Department of Computer Science, The Johns Hopkins University, September 2007. (paper)

[54] J. S. Kim and G. S. Chirikjian. Conformational analysis of stiff chiral polymers with end-constraints. *Molecular Simulation*, 32(14):1139–1154, December 2006. doi:10.1080/08927020601024137. (paper)

[55] D. M. Lane, J. B. C. Davies, G. Robinson, D. J. O'Brien, J. Sneddon, E. Seaton, and A. Elfstrom. The amadeus dextrous subsea hand: design, modeling, and sensor processing. *IEEE Journal of Oceanic Engineering*, 24(1):96–111, 1999. 0364-9059. doi:10.1109/48.740158. (paper)

[56] H. Lang, J. Linn, and M. Arnold. Multibody dynamics simulation of geometrically exact Cosserat rods. In *Multibody Dynamics 2009, ECCOMAS Thematic Conference*, Warsaw, Poland, June 29 - July 2 2009. (paper)

[57] O. Larson and C. Davidson. Flexible arm, particularly a robot arm, 1985. U. S. Patent 4,494,417. (paper)

[58] C. Li and C. Rahn. Design of continuous backbone, cable-driven robots. *ASME Journal of Mechanical Design*, 124(2):265–271, 2002. doi:10.1115/1.1447546. (paper)

[59] L. Lyons, R. J. Webster III, and R. Alterovitz. Motion planning for active cannulas. In *IEEE/RSJ International Conference on Intelligent Robots and Systems*, pages 801–806, St. Louis, MO, USA, October 2009. (paper)

[60] Measurand Inc. http://www.measurand.com/.

[61] H. Mochiyama, E. Shimemura, and H. Kobayashi. Shape control of manipulators with hyper degrees of freedom. *The International Journal of Robotics Research*, 18(6):584–600, 1999. doi:10.1177/02783649922066411. (paper)

[62] M. E. Moran. Evolution of robotic arms. *Journal of Robotic Surgery*, 1(2):103–111, 2007. doi:10.1007/s11701-006-0002-x. (paper)

[63] R. M. Murray, Z. Li, and S. S. Sastry. *A Mathematical Introduction to Robotic Manipulation*. CRC Press, Boca Raton, FL, 1994.

[64] Y. Nakamura, A. Matsui, T. Saito, and K. Yoshimoto. Shape-memory-alloy active forceps for laparoscopic surgery. *IEEE International Conference on Robotics and Automation*, pages 2320–2327, 1995. doi:10.1109/ROBOT.1995.525607. (paper)

[65] S. Neppalli, M. A. Csencsits, B. A. Jones, and I. D. Walker. Closed-form inverse kinematics for continuum manipulators. *Advanced Robotics*, 23:2077–2091, 2009. (paper)

[66] S. Neppalli and B. A. Jones. Design, construction, and analysis of a continuum robot. *IEEE/RSJ International Conference on Intelligent Robots and Systems*, pages 1503–1507, 2007. doi:10.1109/IROS.2007.4399275. (paper)

[67] L. Nocks. *The robot : the life story of a technology.* Greenwood technographies,. Greenwood Press, Westport, Conn., 2007.

[68] H. Ohno and S. Hirose. Study on slime robot (proposal of slime robot and design of slim slime robot). In *Proceedings of the IEEE/RSJ International Conference on Intelligent Robots and Systems*, volume 3, pages 2218–2223, November 2000. doi:10.1109/IROS.2000.895298. (paper)

[69] H. Ohno and S. Hirose. Design of slim slime robot and its gait of locomotion. In *Proceedings of the IEEE/RSJ International Conference on Intelligent Robots and Systems*, volume 2, pages 707–715, November 2001. doi:10.1109/IROS.2001.976252. (paper)

[70] R. Ohta. Results of R&D on catheter-type micromachine. In *International Symposium on Micromechatronics and Human Science*, pages 5–12, 2001. doi:10.1109/MHS.2001.965214. (paper)

[71] K. Osuka and H. Kitajima. Development of mobile inspection robot for rescue activities: MOIRA. In *IEEE/RSJ International Conference on Intelligent Robots and Systems*, pages 3373–3377, 2003. (paper)

[72] E. Paljug, T. Ohm, and S. Hayati. The JPL serpentine robot: a 12-DOF system for inspection. In *IEEE International Conference on Robotics and Automation*, volume 3, pages 3143–3148, May 1995. doi:10.1109/ROBOT.1995.525732. (paper)

[73] J. Park and W.-K. Chung. Geometric integration on Euclidean group with application to articulated multibody systems. *IEEE Transactions on Robotics*, 21(5):850–863, 2005. doi:10.1109/TRO.2005.852253. (paper)

[74] J. Peirs, D. Reynaerts, H. Van Brussel, G. De Gersem, and H. T. Tang. Design of an advanced tool guiding system for robotic surgery. In *IEEE International Conference on Robotics and Automation*, pages 2651–2656, 2003. doi:10.1109/ROBOT.2003.1241993. (paper)

[75] S. J. Phee, W. S. Ng, I. M. Chen, F. Seow-Choen, and B. L. Davies. Locomotion and steering aspects in automation of colonoscopy part one: A literature review. *IEEE Engineering in Medicine and Biology Magazine*, 16(6):85–96, November/Detember 1997. (paper)

[76] K. Reed, V. Kallem, R. Alterovitz, K. Goldberg, A. M. Okamura, and N. J. Cowan. Integrated planning and image-guided control for planar needle steering. In *IEEE RAS/EMBS International Conference on Biomedical Robotics and Biomechatronics*, pages 819 – 824, Scottsdale, AZ, USA, October 2008. (paper)

[77] G. Robinson and J. B. C. Davies. Continuum robots – a state of the art. In *IEEE International Conference on Robotics and Automation*, pages 2849–2854, May 1999. doi:10.1109/ROBOT.1999.774029. (paper)

[78] OC Robotics. Snake-arm robots access the inaccessible. *Nuclear Technology International*, 1:92–94, 2008. (paper)

[79] M. E. Rosheim. *Robot evolution: the development of anthrobotics*. Wiley, New York, N.Y., 1994.

[80] D. C. Rucker, J. M. Croom, and R. J. Webster III. Aiming surgical lasers with an active cannula. *ASME Journal of Medical Devices*, 3(2):027506, 2009.

[81] D. C. Rucker, B. A. Jones, and R. J. Webster III. A geometrically exact model for externally loaded concentric tube continuum robots. *IEEE Transactions on Robotics*, 2010. (Accepted).

[82] D. C. Rucker and R. J. Webster III. Mechanics-based modeling of bending and torsion in active cannulas. *IEEE RAS/EMBS International Conference on Biomedical Robotics*

and Biomechatronics, pages 704–709, 2008. doi:10.1109/BIOROB.2008.4762918. (paper)

[83] D. C. Rucker and R. J. Webster III. Mechanics of bending, torsion, and variable precurvature in multi-tube active cannulas. *IEEE International Conference on Robotics and Automation*, pages 2533–2537, 2009. (paper)

[84] D. C. Rucker and R. J. Webster III. Parsimonious evaluation of concentric-tube continuum robot equilibrium conformation. *IEEE Transactions on Biomedical Engineering*, 56(9):2308–2311, 2009. (paper)

[85] D. C. Rucker, R. J. Webster III, G. S. Chirikjian, and N. J. Cowan. Equilibrium conformations of concentric-tube continuum robots. *International Journal of Robotics Research*, 2010. (In Press).

[86] P. Sears and P. E. Dupont. A steerable needle technology using curved concentric tubes. In *IEEE/RSJ International Conference on Intelligent Robots and Systems*, pages 2850–2856, Beijing, China, October 2006. doi:10.1109/IROS.2006.282072. (paper)

[87] P. Sears and P. E. Dupont. Inverse kinematics of concentric tube steerable needles. In *IEEE International Conference on Robotics and Automation*, pages 1887–1892, April 2007. doi:10.1109/ROBOT.2007.363597. (paper)

[88] N. Simaan. Snake-like units using flexible backbones and actuation redundancy for enhanced minaturization. In *IEEE International Conference on Robotics and Automation*, pages 3023–3028, Barcelona, Spain, April 2005. (paper)

[89] N. Simaan, R. Taylor, and P. Flint. A dexterous system for laryngeal surgery. In *IEEE International Conference on Robotics and Automation*, pages 351–357, April 2004. doi:10.1109/ROBOT.2004.1307175. (paper)

[90] N. Simaan, K. Xu, W. Wei, A. Kapoor, P. Kazanzides, R. Taylor, and P. Flint. Design and integration of a telerobotic system for minimally invasive surgery of the throat.

The International Journal of Robotics Research, 28(9):1134–1153, 2009. doi:10.1177/0278364908104278. (paper)

[91] J. Spillmann and M. Teschner. Corde: Cosserat rod elements for the dynamic simulation of one-dimensional elastic objects. In *SCA '07: Proceedings of the 2007 ACM SIGGRAPH/Eurographics symposium on Computer animation*, pages 63–72, Aire-la-Ville, Switzerland, 2007. (paper)

[92] J. Suthakorn and G. S. Chirikjian. A new inverse kinematics algorithm for binary manipulators with many actuators. *Advanced Robotics*, 15(2):225–244, 2001. doi:10.1163/15685530152116245. (paper)

[93] K. Suzumori, S. Wakimoto, and M. Takata. A miniature inspection robot negotiating pipes of widely varying diameter. *IEEE International Conference on Robotics and Automation*, pages 2735–2740, 2003. (paper)

[94] M. Takahashi, I. Hayashi, N. Iwatsuki, K. Suzumori, and N. Ohki. The development of an in-pipe microrobot applying the motion of an earthworm. *International Symposium on Micro Machine and Human Science*, pages 35–40, 1994. doi:10.1109/ISMMHS.1994.512895. (paper)

[95] E. Tatlicioglu, I. D. Walker, and D. M. Dawson. New dynamic models for planar extensible continuum robot manipulators. In *Proceedings of the 2007 IEEE/RSJ International Conference on Intelligent Robots and Systems*, pages 1485 – 1490, 2007. (paper)

[96] M.W. Thring. *Robots and Telechirs; Manipulators with Memory; Remote Manipulators; Machine Limbs for the Handicapped*. Ellis Horwood, 1983.

[97] A. A. Transeth, K. Y. Pettersen, and P. Liljeback. A survey on snake robot modeling and locomotion. *Robotica*, 2009. doi:10.1017/S0263574709005414. (paper)

[98] D. Trivedi, A. Lotfi, and C. D. Rahn. Geometrically exact models for soft robotic manipulators. *IEEE Transactions on Robotics*, 24(4):773–780, August 2008. doi:10.1109/TRO.2008.924923. (paper)

[99] D. Trivedi, C. D. Rahn, W. M. Kierb, and I. D. Walker. Soft robotics: Biological inspiration, state of the art, and future research. *Applied Bionics and Biomechanics*, 5(3):99117, 2008. doi:10.1080/11762320802557865. (paper)

[100] H. Tsukagoshi, A. Kitagawa, and M. Segawa. Active hose: an artificial elephant's nose with maneuverability for rescue operation. In *Proceedings of the IEEE International Conference on Robotics and Automation*, volume 3, pages 2454–2459, Seoul, Korea, 2001. doi:10.1109/ROBOT.2001.932991. (paper)

[101] Y. Wakahara, K. Asano, and T. Tsuchihashi. A computer aided manipulation system for a multijoint inspection robot. *Transactions of the American Nuclear Society*, 47:455–456, 1984.

[102] R. J. Webster III. *Design and Mechanics of Continuum Robots for Surgery*. Mechanical engineering, The Johns Hopkins University, Baltimore, MD, December 2007. PhD Thesis. (paper)

[103] R. J. Webster III, J. S. Kim, N. J. Cowan, G. S. Chirikjian, and A. M. Okamura. Nonholonomic modeling of needle steering. *International Journal of Robotics Research*, 25(5/6):509–526, May/June 2006. doi:10.1177/0278364906065388. (paper)

[104] R. J. Webster III, J. Memisevic, and A. M. Okamura. Design considerations for robotic needle steering. *IEEE International Conference on Robotics and Automation*, pages 3599–3605, 2005. (paper)

[105] R. J. Webster III, A. M. Okamura, and N. J. Cowan. Toward active cannulas: Miniature snake-like surgical robots. *IEEE/RSJ International Conference on Intelligent Robots and Systems*, pages 2857–2863, 2006. doi:10.1109/IROS.2006.282073. (paper)

[106] R. J. Webster III, J. M. Romano, and N. J. Cowan. Mechanics of precurved-tube continuum robots. *IEEE Transactions on Robotics*, 25(1):67–78, 2009. doi:10.1109/TRO.2008.2006868. (paper)

[107] R. J. Webster III, J. P. Swenson, J. M. Romano, and N. J. Cowan. Closed-form differential kinematics for concentric-tube continuum robots with application to visual servoing. *11th International Symposium on Experimental Robotics 2008, Springer Tracts in Advanced Robotics.*, 54:485–494, 2008. (paper)

[108] J. F. Wilson, D. Li, Z. Chen, and Jr. R. T. George. Flexible robot manipulators and grippers: Relatives of elephant trunks and squid tentacles. In Paolo Dario, Giulio Sandini, and Patrick Aebischer, editors, *Robots and Biological Systems: Towards a New Bionics?*, volume 102 of *NATO ASI Series*, pages 475–494. Springer, 1993.

[109] A. Wolf, H. B. Brown, R. Casciola, M. Schwerin A. Costa, E. Shamas, and H. Choset. A mobile hyper redundant mechanism for search and rescue tasks. *IEEE/RSJ International Conference on Intelligent Robots and Systems*, pages 2889–2895, 2003. doi:10.1109/IROS.2003.1249309. (paper)

[110] C. Wright, A. Johnson, A. Peck, Z. McCord, A. Naaktgeboren, P. Gianfortoni, M. Gonzalez-Rivero, R. Hatton, and H. Choset. Design of a modular snake robot. In *Proceedings of the 2007 IEEE/RSJ International Conference on Intelligent Robots and Systems*, pages 2609–2614, 2007. doi:10.1109/IROS.2007.4399617. (paper)

[111] K. Xu and N. Simaan. Actuation compensation for flexible surgical snake-like robots with redundant remote actuation. *IEEE International Conference on Robotics and Automation*, pages 4148–4154, 2006. doi:10.1109/ROBOT.2006.1642340. (paper)

[112] K. Xu and N. Simaan. An investigation of the intrinsic force sensing capabilities of continuum robots. *IEEE Transactions on Robotics*, 24(3):576–587, June 2008. doi:10.1109/TRO.2008.924266. (paper)

View publication stats